Development of P-I Diagrams for Framed PVB-Laminated Glass Windows

Development of P-I Diagrams for Framed PVB-Laminated Glass Windows

Suwen CHEN [1], Xing CHEN [2], Guo-Qiang LI [3], Yong LU [4]

[1] Professor, State Key Laboratory of Disaster Reduction in Civil Engineering, Tongji University, Shanghai 200092, China

[2]Phd student, College of Civil Engineering, Tongji University, Shanghai 200092, China

[3] Professor, College of Civil Engineering, Tongji University, Shanghai 200092, China

[4]Professor, Institute for Infrastructure and Environment, School of Engineering, The University of Edinburgh, Edinburgh EH9 3JL, UK

ABSTRACT

In this paper, iso-damage criteria for framed PVB-laminated glass panel subjected to blast load are investigated. The iso-damage criteria are presented in the form of pressure-impulse (P-I) diagrams, and a methodology for the generation of the P-I diagrams for laminated glass is developed based on numerical simulation studies and the energy method. Three damage levels are classified in accordance with the conditions identified in GSA/ISC, namely (I) glass crack limit, (II) PVB rupture limit, and (III) overall detachment with a specific velocity after PVB ruptures. Based on nonlinear finite element analysis, the governing failure modes of the glass panel in both impulsive and quasi-static regions for each damage level are identified and the corresponding deflection functions are determined. Especially, a simplified PVB tensile bar model is proposed to describe the local tensile failure of PVB laminated glass corresponding to damage level III under impulsive loading. On the above basis, the pressure and impulse asymptotes of framed PVB-laminated glass for different damage levels are derived using the energy balance principle. The proposed method is validated through comparison with published experimental data and further numerical results. This method can provide a reference for engineering design and hazard estimation of framed PVB-laminated glass against blast loading and can be extended to laminated glazing with other interlayers.

Keywords: Framed glass window; PVB-laminated glass; blast loading; P-I diagram; failure modes; analytical method

30 **NOMENCLATURE**

31

i_{cr}^{k} , p_{cr}^{k}	values of impulse asymptote and overpressure asymptote for damage level k, respectively
k	damage level, k = I, II, III…
α, β	shape parameters for the dynamic region of P-I curve
a, b	length and width of the glass panel, with $a \geq b$
h_g	thickness of single glass ply
h_i	thickness of PVB interlayer
E_g	elastic modulus of glass
E_i	elastic modulus of PVB
E_i^*	equivalent modulus of cracked laminated glass panel
v_g	Poisson's ratio of glass
v_i	Poisson's ratio of PVB
m^*	equivalent mass of pre-crack laminated glass panel
D^*	equivalent bending stiffness of pre-crack laminated glass panel
$\varepsilon_x, \varepsilon_y, \gamma_{xy}$	strain components
σ_f	failure stress of glass material
ε_f	failure tensile strain of the cracked laminated glass
c_1, c_2	undetermined parameters in the deflection function
ψ^k	deflection function for damage level k
w	deflection at the panel centre
w_f^k	deflection at the panel centre of the final state of damage level k
p	peak overpressure of a specific blast load
i	impulse of positive phase of a specific blast load
t_d	equivalent positive load duration of a specific blast load
D_s	width of damage region
C	total length of damage region
M_e^k	equivalent mass of the equivalent model for damage level k
K_e^k	equivalent stiffness of the equivalent model for damage level k
P_e^k	equivalent load of the equivalent model for damage level k
W^k	the external work for damage level k
σ_1	maximum principal stress within the uncracked glass panel
V_0^k	initial kinetic energy of laminated glass panel for damage level k
V_r	residual kinetic energy

v_0^k	initial velocity at the panel centre for damage level k
v_r	ejection velocity at the centre of the detached laminated glass
U_i^k	internal strain energy of the laminated glass panel for damage level k
λ	ratio of residual kinetic energy to total energy at glass failure moment
λ_c	critical residual kinetic energy ratio for local tensile failure mode
v_{rc}	critical ejection velocity for local tensile failure mode
ξ	linear transition index

1. INTRODUCTION

As the envelope of a building, glass windows are immediately exposed to blast loading in the event of an explosion. Normal glass windows would offer very little resistance against blast due to the brittle nature of glass materials, and high speed glass debris can cause severe injures (Norville et al. 1999). To mitigate the hazard of glass fragment ejection, laminated glass is widely used in public and high-rise buildings as a kind of safety glass. Laminated glass is generally composed of multiple sheets of glass bonded together by interlayers. As such, when the glass fractures, the glass fragments will be retained on the interlayer. Moreover, the interlayer can still dissipate blast energy through large deformations, therefore it can effectively protect indoor occupants.

To assist blast resistant design for glass windows, several test standards (GSA-TS01 2003; ISO 16933 2007; ISO 16934 2007; BS EN 13541 2012) and design guidelines (ASTM-E1300 2012; UFC 4-010-01 2013) have been developed. For example, the GSA-TS01 (2003) standard is mainly concerned about estimating the performance of window systems subjected to blast loads. Hazard levels are categorized in this standard according to the responding conditions of the window system, as indicated in Figure 1. These conditions are specified based upon the state of the glass window and the location of fragments and debris relative to the original location of the window. For condition 1 there should be no visible damage, and for condition 2 the glazing can crack but is retained by the frame and only dusting or very small fragments near sill or on floor should occur. Condition 3a to 5 are classified according to different invasion distances and corresponding hazard levels. The UFC 4-010-01 (2013) standard specifies the minimum thickness of

laminated glass to provide a minimum level of protection against blast threat. A more generalized design approach has been introduced in the ASTM-E1300 (2012) standard. Design charts for determining the load resistance of different types of glass windows are provided, and can be used for the blast resistant design together with ASTM-F2248 (2012), which specifies a 3-second duration equivalent design load. It should be noted that the load resistance provided in ASTM-E1300 (2012) is associated with a breakage probability up to 8 lites per 1000, therefore the design goal of this standard corresponds to condition 1 in GSA/ISC (2003), which is the glass crack limit. As laminated glass can still offer great resistance after glass fractures, the blast resistance capacity of laminated glass is apparently underestimated if the post-crack stage is not taken into account.

The pressure–impulse (P–I) diagram provides another useful tool for preliminary blast resistant design and hazard assessment. It was firstly developed to evaluate building damage in bomb attacks in the UK (Jarrett D.E. 1968; Cormie et al. 2009), and was then extended to structural component damage (Biggs 1964; Li and Meng 2002; Cormie et al. 2009) and human injuries (Baker 1983; Merrifield R. 1993; Hetherington and Smith 1994). Figure 2 shows the primary features of a P-I diagram, in which i_{cr}^{k} and p_{cr}^{k} are the critical impulse and the critical overpressure for a given failure level k respectively. Three typical regions, corresponding to impulsive loading, dynamic loading and quasi-static loading, respectively, are classified in a P-I diagram.

A range of research studies, including analytical derivation and numerical simulation, have been devoted to develop P-I curves with different damage levels for laminated glass. For example, a SDOF model is developed by Cormie et al. (2009), in which the pre-crack and post-crack resistance functions are derived with the classic large deformation plate theory and the membrane analysis, respectively. Using the combined resistance function together with the equivalent load-mass transformation factor, time history analyses can be carried out with the equivalent SDOF model for design blast loadings. Then the P-I curves corresponding to specific failure criteria can be generated. Hooper et al. (2012) employed numerical analysis and established P-I curves for a 7.52mm-thick 1.5m×1.2m laminated glass. The P-I curves obtained were compared with the predictions using the above-mentioned SDOF model. The results show considerable error in the values of the impulse asymptote for the glass crack limit, and this error was attributed to the non-

uniformity of the pressure distribution in the impulse region that was not properly considered in the SDOF model. Zhang et al. (2013) derived empirical formulae based on numerical parametric calculations to predict the pressure and impulse asymptotes as functions of interlayer thickness, glass thickness and panel dimension for the PVB rupture limit. Good agreement was achieved when comparing the results with those from Cormie et al. (2009) and Hooper et al. (2012).

In spite of the above progresses on developing P–I diagrams for laminated glass in the recent years, several issues remain to be addressed, and in particular:

1) The commonly used SDOF method assumes a deflection shape based only upon the first mode of vibration. This assumption is known to apply in cases of quasi-static loading (Cormie et al. 2009), but under blast loading higher modes of vibration may be excited, resulting in a different deflection mode and stress distribution (Shi et al. 2008; Spiller et al. 2016). Therefore, the current SDOF method may not always yield reliable predictions, especially for failure modes like punching shear (local failure mode).

2) Published studies mainly consider a glass crack limit and a PVB rupture limit when developing P-I curves for laminated glass, which correspond to condition 1 and 2 in GSA/ISC (2003) standard. P-I curves corresponding to condition 3a-5 specified in GSA/ISC (2003) are also needed for more diverse design requirements and solutions.

This paper is concerned with the development of P-I curves for different damage levels of framed PVB-laminated glass subjected to blast loading. Three typical damage levels corresponding to different conditions in GSA/ISC are classified, namely a) glass crack limit, b) PVB rupture limit, and c) overall detachment with a specific velocity after PVB ruptures. For laminated glass, most of glass fragments can be retained by the interlayer after glass fracture, while some may fly inside and can correspond to condition 3a-5 in GSA/ISC (2003). It should be noted that the above case is not the main concern of this paper. On the other hand, due to the differences in glass-frame connection in practical engineering, the effectiveness of clamping cannot be guaranteed. Under blast loading, the cracked laminated glass can develop horizontal deflections due to large vertical deformation (geometric non-linearity), and consequently the cracked laminated glass panel may be pulled out in one big piece without PVB rupture if it is not properly glued to the frame. In this study, the laminated glass is assumed to be fully gripped within the frame with silicone

cushion, and pull-out failure is not considered.

Based on numerical analysis, the failure modes and deflection functions for the critical states of the above-mentioned three different damage levels are analysed and determined. A simplified PVB tensile bar model is proposed to describe the punching-type failure of PVB laminated glass corresponding to damage level III under impulsive loading. The width of the damage region, which is a key parameter in the PVB tensile bar model, is analysed numerically, and an empirical formula is derived for this parameter based on numerical parametric analysis. Then energy method is adopted to theoretically derive the pressure asymptote and impulse asymptote of P-I curves, while the dynamic region of P-I curves is established in an empirical manner based on numerical analysis results. The generated P-I curves are compared with published experimental results, numerical results and the empirical predictions from other researchers to validate the proposed method for building P-I curves. The proposed method enables the development of P-I curves for quick estimation of the damage state and invading distance for an existing design, as well as for a new design to meet a required level of protection.

2. FINITE ELEMENT MODEL FOR NUMERICAL INVESTIGATIONS

In this section, a 3D-solid FE model is developed for simulating laminated glass subjected to blast loading using LS-DYNA. It should be noted that various FE-models, such as layered model, smear model, 3D-solid model have been developed for simulating the behaviour of laminated glass subjected to blast loading (Timmel et al. 2007; Weggel and Zapata 2008; Larcher et al. 2012; Zhang et al. 2013; Nawar et al. 2015; Pelfrene et al. 2016). As is pointed out by Larcher et al. (2012), 3D-solid model is capable of providing the most detailed results although it is computationally more time-consuming. In this respect, a 3D-solid modelling approach is employed for FE analysis in the present study. The model is validated against published experimental data and then used for further numerical analyses on the failure modes as presented in Section 3.

2.1 Boundaries and elements

Figure 3a shows the geometry of the FE model. The glass panel is of typical laminated glazing with thickness of 7.52mm (3+1.52+3mm). The plane size of the glass panel is 1500mm ×1200mm.The laminated panel is fully gripped within the steel frame with 50mm embedment on all four sides, and the thickness of steel plate is 5mm. According to engineering practice, a 2mm-thick silicone cushion is inserted between the frame and the glass panel. The nodes on the outer surface of the frame are restrained in all directions to simulate a fix boundary condition. It should be noted that the assumed boundary condition is only suitable for stiff supporting systems. The model does not cover cases where a soft supporting system is utilized, as in those cases the deflection of the sub-structure may develop and subsequently influence the dynamic response and failure modes of the laminated glass panels. To simulate the adhesion of silicone cushion, the nodes at the silicone-frame interface and silicone-glass interface are merged together (i.e. shared nodes) respectively. The debonding of silicone sealant is not considered, but in principle failure of bond can still be captured through the failure of silicone material.

In the FE model, the inner and outer glass plies are each meshed with 3 elements across the thickness to simulate their separate bending effect, while the middle PVB interlayer is meshed into just one layer along the thickness, as shown in Figure 3b. An 8-node solid element (Solid164) with one-point integration is adopted for all parts of the framed glass. It should be mentioned that while the single-integration scheme is well suited for the explicit dynamic analysis adopted in this study and can significantly save computing time, the zero-energy mode (“hourglass”) could be introduced by this scheme, resulting in unrealistic simulation results. To mitigate such an effect, an appropriate hourglass control is needed. In this study, a viscosity type (node velocity-based) hourglass force vector is introduced to inhibit the hourglass deformation during numerical calculation. The adopted hourglass control mode is especially suitable for high strain rate problems such as under blast loading (LS-DYNA Keyword user's manual 2007). On the other hand, the meshing size can also influence the simulation result. Based on a preliminary mesh convergence study, an element size of 5mm in both X and Y directions is found to provide a stabilised outcome, in that further reduction of the mesh size would only introduce a negligible improvement of the numerical results but lead to a substantial increase in the computing time.

2.2 Material models

The material properties employed in the FE analysis are listed in Table 1. Glass is a kind of elastic brittle material, therefore, the material type "ELASTIC" is adopted for glass (Weggel and Zapata 2008; Ge 2012; Larcher et al. 2012; Nawar et al. 2015; Chen et al. 2016; Pelfrene et al. 2016) with a stress failure criterion. The corresponding elastic modulus, Poisson's ratio and mass density of glass are taken as E = 72GPa, $v = 0.22$ and $\rho = 2560$ kg/m^3 respectively.

The PVB material considered in this study is typical architectural adoptive PVB. A strain rate dependent elastic-plastic material model is adopted for PVB interlayer considering that it behaves elastoplastically when subjected to high strain rate tensile load (Bennison et al. 2005; Iwasaki et al. 2007; Chen et al. 2015; Zhang et al. 2015). The strain rate dependent yield stress and initial Young's modulus for PVB given by Zhang et al. (2013) are adopted:

$$\sigma_{yield} = 2.167(\dot{\varepsilon})^{0.399} \text{ MPa}$$

$$E_{initial} = 30.591(\dot{\varepsilon})^{0.271} \text{ MPa}$$

A constant plastic modulus of 11MPa is adopted for PVB (Zhang et al. 2013).

The silicone sealant used in structural glass applications is typically an uncompressible hyper elastic material with low modulus of elasticity, limited tensile/shear resistance and large ultimate strain (Larcher et al. 2016). Several material models have been adopted for silicone sealant in numerical modelling. Under low strain rate, silicone sealant exhibits the same material property as rubber, which can be considered as a hyper-elastic material (Pelfrene et al. 2016). Under high strain rate, the silicone sealant also shows "elastic–plastic" behaviour and can be considered as an elastoplastic material (Hidallana-Gamage et al. 2014). There are also studies adopting linear elastic material to simplify the numerical modelling scheme (Weggel and Zapata 2008; Larcher et al. 2012; Weggel et al. 2013; Nawar et al. 2015), while still producing satisfactory results. In this study, an elastic material model is used for silicone sealant with a Young's modulus of 3.5 MPa (Larcher et al. 2012), and the corresponding Poisson's ratio and mass density are taken as $v = 0.495$ and $\rho = 1000$ kg/m^3 respectively.

186

187 2.3 Simulation of material failure

188

189 To simulate glass crack and PVB rupture, the erosion technique in LS-DYNA is utilized. The erosion
190 limit for glass is defined by the principal stress, such that an element will be deleted when its first principal
191 stress reaches 80MPa (Hooper et al. 2012). It should be noted that the strain rate effect can be important for
192 the fracture of brittle material like annealed glass due to the fact that the growths of micro-crack need time.
193 Results from dynamic split tensile tests show that the tensile strength increase significantly when the strain
194 rate is very high (over $300s^{-1}$) (Zhang et al. 2012). Nevertheless, as will be discussed later, the strength of the
195 glass is only important in the level I damage case, i.e. the glass crack limit, for which the governing mode
196 would be global bending and hence should not involve high strain rate. Therefore, the strain rate effect on
197 the glass material is ignored, and a constant failure stress of 80MPa is employed. For PVB interlayer, the
198 erosion is triggered by rupture using the strain failure criterion. Some available data obtained from uniaxial
199 tensile tests have been summarized by Zhang et al. (2015), and it can be found that the engineering failure
200 strain mainly vary in the range of 1.5~2.8, and it shows a slight decrease with respect to the rise of strain
201 rate. By taking the average value of experimental data, the failure strain (converted into true strain) of PVB
202 is taken as 1.2 uniformly for different strain rates. The true failure strain of silicone is taken as 1.6 (Larcher
203 et al. 2016). Since this study mainly focuses on the dynamic behaviour of the laminated glass panel, the
204 failure of steel frame is not considered.

205 It should be noted that, in spite of its effectiveness, the above modelling method with erosion may
206 not precisely capture the details of the fracture of glass and may result in “unrealistic” glass crack patterns.
207 Understandably the predicted crack pattern thus also depends on the meshing when using element deletion.
208 Nevertheless, the influence of meshing topology has been found to be insignificant on the overall response
209 of a four-side clamped laminated glass when subjected to blast loading (Pelfrene et al. 2016). Therefore the
210 modelling approach is considered as appropriate concerning the global dynamic response and the failure
211 modes of laminated glass panel, which form the basis of proposing the analytical model of the P-I curves.

212

213 2.4 Simplified blast loading

214

215 A simplified triangular decay overpressure time history is adopted in the current analysis and assumed to be
216 uniformly distributed on the panel. In a typical blast load scenario, the blast overpressure rapidly rises to the
217 peak positive pressure, and then gradually reduces until it reaches the peak negative pressure, and finally it
218 returns back to the ambient pressure slowly, as shown in Figure 4. Based on impulse equivalence, a
219 triangular decay function is obtained by equating the triangle area to the original positive impulse. In this
220 study the negative phase of blast loading is ignored.

221 It should be noted that some previous studies show that the negative phase may have a significant
222 influence in situations where the rebound occurs during the negative phase (Krauthammer and Altenberg
223 2000; Wei and Dharani 2005, 2006), leading possibly to pull-out failure under the combined effect of the
224 elastic recovery force and the negative phase of the loading. On the other hand, further study shows that the
225 influence of negative phase on the peak response varies with structure properties and is negligibly small for
226 a stiff system (Teich and Gebbeken 2010). Besides, as is pointed out by Hidallana-Gamage et al. (2017), the
227 negative phase has a negligible impact on the centre deflection, energy absorption and the support reactions
228 of laminated glass panels with rigid supports. In this study, and the upper and bottom surfaces of the steel
229 frame are restrained in all directions to simulate a fixed boundary condition, as such the effect of the
230 negative phase would be insignificant and is ignored.

231 On the other hand, a simplified uniformly distributed overpressure is adopted in both theoretical
232 analysis and numerical simulation as a generic representation in this study. It should be noted that the blast
233 loading may be non-uniformly distributed for close range explosions due to the variation in blast shock wave
234 propagation distances and incident angles at different location over the panel. However, a very-close range
235 explosion may lead to the destruction of structural members, in which case the failure of glazing is not a
236 primary concern. Therefore a uniform blast pressure is considered suitable for the general analysis of glass
237 panels in the present study.

238

239 2.5 Validation of the numerical model

In order to validate the FE model described above, numerical simulations have been conducted for the blast tests reported by Hooper et al. (2012), in which eight 1500mm × 1200mm × 7.52mm laminated glass specimens (two layers of 3 mm float glass and a 1.52 mm PVB interlayer) were tested. The reflected pressure was measured using a pressure sensor located at the centre of the window. The deflection profile and the failure process of the panel were monitored using the high-speed 3D digital image correlation technique.

Two of Hooper's tests are simulated for validation of the present FE model, and the recorded blast loadings (positive phase) are listed in Table 2. Figure 5 shows the comparison of the deflection profiles from the tests and the FE simulations. For the test case with 15kg TNT at 13m, the maximum deflection at the panel centre is 173mm from the test and 167mm from the numerical result, giving a difference of only 3.5%. The overall deflection profiles predicted by current FE model agree well with the experimental profiles at different steps of the response. For the other test with 15kg TNT at 10m, the deflection profiles from the test and the numerical simulation also show good agreement until the central displacement reaches a large deflection of about 150mm. At t = 9ms, the maximum deflection from the test result is 180mm, and the FE prediction is 160 mm, giving a difference of 12.2%. After that the experimental deflections become much larger than the FE results. As can be observed in the figure, the difference should be mainly attributed to the deviations close to the edge. In Hooper's test (2012), the laminated glass was bonded on all four edges to a steel sub-frame with a 6-mm thick single-sided silicone joint and a nominal bonding depth of just 20 mm. Therefore considerable deformation developed in the silicone joint and even failed in the case with 15kg TNT at 13m (after t = 9ms), allowing large displacements at the edges. However, in the present analysis, both sides of the laminated glass are bonded with the frame through silicone cushion and a larger bonding depth of 50mm is adopted to simulate the clamped boundary condition. The deflection of laminated glass at the frame edges is negligibly small, and no silicone failure occurs in the numerical simulation. Since difference exists in the boundary conditions of the current FE model with Hooper's tests, the model is not directly validated. Nevertheless, the above comparisons demonstrate that the current FE model can produce satisfactory predictions of the dynamic response of laminated glass panel under blast loading for a stiff and

well clamped system.

3. ANALYSIS OF FAILURE MODES OF LAMINATED GLASS

The validated FE model described in Section 2 is employed to analyze the failure modes of representative laminated glass subjected to different blast loadings and establish the deflection functions for the critical states of three different damage levels. These deflection functions can provide the basis for establishing the asymptotes in the P-I diagrams.

3.1 FAILURE MODE AND DEFLECTION FUNCTION IN IMPULSE REGION

An impulsive loading is featured by a very high peak overpressure and a very short load duration (t_d) comparing with the natural period of the structure (T). It is generally understood that when the duration of the load is less than one-tenth of the natural period of the structure (the glass panel herein), i.e., $t_d/T \leq 0.1$, the response level will be dominated mainly by the impulse rather than the peak load or duration separately (Cormie et al. 2009). For this reason, and considering that in the blast resistance design for glazing the peak overpressure is relatively small comparing with those for main structural members, in the current numerical study a constant peak overpressure of 1000kPa is adopted for impulsive loading. The magnitude of the loading as measured by the impulse varies with the load duration. As the natural period of the representative PVB-laminated window is approximately 24ms, the load durations are varied within 2ms ($t_d \leq 2$ms) to ensure an impulsive loading condition.

Observations from preliminary numerical analysis indicate that for different damage levels the governing deflection mode of the glass panel is different even within the impulsive loading region. As shown in Figure 6, in general the governing mode changes from global failure to local failure with the increase of the impulse (from 25kPa·ms to 700kPa·ms herein). This phenomenon is crucial for the theoretical formulation, therefore the governing modes of response and failure in the impulsive load region will be examined in detail in following subsections.

294

295 3.1.1 Damage level I

296

297 The threshold for damage level I for impulse region, i.e. fracture of glass, is i = 25kpa·ms, which effectively
298 defines the impulse asymptote for this damage level. In this case, cracks initially occur along the boundaries,
299 and subsequent cracks develop around the centre of the glass panel as a result of global bending
300 deformation. Figure 7 shows the development of the deflection profiles from the numerical results. As can
301 be seen, at the beginning, the deformation of the laminated glass mainly concentrates near the boundaries
302 due to impulsive load. As the impulse is not large enough to cause a direct punching-style shear failure, the
303 response of the panel develops into a global deformation stage, resulting in flexural failure at t = 2.5 ms.

304 It is worth noting that for a loading with an impulse below the above threshold, for example i =
305 15kPa·ms (peak overpressure remains at p = 1000 kPa), the deflection path goes through a similar process
306 but no crack occurs in the early punching phase, and nor at the final bending stage. On the other hand, for a
307 loading with a larger impulse than the threshold, e.g. i = 40 kPa·ms, the glass fails at early deformation
308 stage. Figure 8 shows a comparison of the kinetic energy and internal strain energy time histories from
309 numerical results for these three loading cases. The time histories are cut off at the time when glass failure
310 occurs for each case, when the deflection shapes are also shown. As can be seen, when the imposed impulse
311 is larger than the threshold for the glass crack limit, the glass failure occurs earlier and the corresponding
312 deformation mainly concentrates along the edge while the deformation in the central region is negligible.
313 The kinetic energy at this moment remains high, which is 17.5 J comparing to the strain energy of 12 J. On
314 the other hand, for the threshold loading with i = 25 kPa·ms the glass survives the early shear phase and
315 eventually goes into global bending stage with flexural crack. At this moment, almost the entire energy of
316 the system is transformed into the internal strain energy, which is about 17.2 J. The above results indicate
317 that the required energy to activate punching failure mode would be larger than that of a global bending
318 failure mode. Therefore global bending is the governing mode for the glass crack threshold.

319 The deflection shape at glass failure threshold matches well the classical plate theory for a four-side
320 fixed plate (Timoshenko 1940), which can be expressed as:

$$\psi^{I}(x,y)=\cos^2(\frac{\pi x}{a})\cos^2(\frac{\pi y}{b}),\ -\frac{a}{2}\le x\le\frac{a}{2},\ -\frac{b}{2}\le y\le\frac{b}{2} \tag{1}$$

The above deflection function will be used in the later derivation of the impulse asymptote for damage level I (glass crack limit).

3.1.2 Damage level II

Damage level II is marked by the initiation of the PVB rupture. In the numerical analysis for the impulsive region, the threshold is identified by gradually increasing the impulse of the load while still keeping the peak overpressure at 1000 kPa, and it is reached when the imposed impulse is 400 kPa·ms. The mode of failure can be observed from Figure 6. Dense glass cracks are formed near the boundaries due to the initial shear force. At the same time, cracks parallel to the boundary lines also appear in the panel central region as a result of global bending deformation. Due to the cohesive effect of the PVB interlayer, the cracked laminated glass panel still deflects as a whole. However, as the cracked glass cannot provide bending stiffness, the whole panel acts more like a "membrane". The bearing capacity is mainly provided by the tension of the PVB membrane between glass fragments, and finally results in tensile failure of PVB. Examining the deflection histories (Figure 9), it is observed that the cracked laminated glass gradually enters into global deformation, and tensile failure of PVB interlayer occurs at t=13ms. Although the glass can never be completely and uniformly fragmented, the final deflection profile at PVB rupture moment shows satisfactory smoothness. Therefore for a theoretical analysis of damage level II (PVB rupture limit), it will be reasonable to assume a deflection function as a rectangular membrane with all four-side fixed, which can be expressed as (Timoshenko 1940):

$$\begin{aligned}\psi_1^{II}(x,y)&=c_1\cos\frac{\pi x}{a}\cos\frac{\pi y}{b}\\ \psi_2^{II}(x,y)&=c_2\sin\frac{2\pi x}{a}\cos\frac{\pi y}{b}\\ \psi_3^{II}(x,y)&=c_2\sin\frac{2\pi y}{b}\cos\frac{\pi x}{a}\end{aligned} \tag{2}$$

where ψ_1^{II}, ψ_2^{II} and ψ_3^{II} represent the displacement distribution for out-of-plane and two in-plane directions, respectively. $c_1$and c_2 are parameters to be determined, in which the same parameter c_2 is adopted for two in-

plane directions for a simplified calculation.

3.1.3 Damage level III

For the fractured laminated glass to break away with a certain velocity, i.e., in damage level III, further increased impulse is required. From the previous cases with damage level I and II, it can be expected that failure would occur early in the early local deformation stage and the failure mode is likely to be dominated by tearing of PVB interlayer near the boundaries. Figure 10 shows the failure process of the laminated glass panel in this mode, and the corresponding blast loading is i = 700 kPa·ms and p = 1000 kPa. As can be seen, under such strong impulsive loading, dense cracks of glass are formed near the boundaries and a "belt" of damage zone develops along the boundary sides. Large tensile deformation is then developed in the damage zone due to an almost total loss of stiffness after glass fracture, while the deformation in the central region appears to be negligible. Gross PVB ruptures along the boundaries occur at t = 2.4 ms and finally the whole laminated panel detaches from the supporting frame at a speed of about 25 m/s.

Similar patterns of failure are observed for other degrees of response in damage level III, i.e., with different ejection velocities. The failure is associated with punching failure and it develops in a very rapid manner which allows no time for the panel to develop global deformation. The final detachment of laminated glass panel is mainly caused by the local tensile failure of PVB interlayer near the boundaries. Under this condition, only a fraction of the impact energy is dissipated by the fracture of glass and PVB near the boundary while the main part carries the kinetic energy corresponding to the ejection of the whole detached panel. To describe this punching-type of failure, a simplified PVB tension bar model is proposed in the present study, which will be detailed in Section 4.2.

It should be pointed out that a mixed failure mode exists between global tensile failure for impulsive loading under damage level II and local tensile failure for impulsive loading under damage level III. As illustrated in Figure 11, if the imposed impulse (i = 550 kPa·ms in this case) is not large enough to cause initial local PVB tensile failure near the boundaries, the deformation mode will transform gradually from local deformation to global deformation subsequently. Mixed failure occurs during the transition process.

370 The extent to which mixed failure will occur is believed to rely on the imposed impulse and the resulting
371 ejection velocity, and a numerical parametric study will be carried out later in section 4.3 to draw a line
372 between local tensile failure and the mixed failure.
373
374 3.2 FAILURE MODE AND DEFLECTION FUNCTION IN QUASI-STATIC REGION
375
376 In the blast loading cases with large standoff distance, the overpressure is relatively small and decreases
377 slowly, resulting in long loading duration and hence a "quasi-static" loading effect. The response of a
378 laminated glass under quasi-static loading will exhibit a similar pattern as under static loading, as depicted in
379 Figure 12. When the imposed overpressure is close to the overpressure asymptote for damage level I (glass
380 crack limit), herein with p=10 kPa and i=10000 kPa·ms (note that the impulse value does not really matter in
381 the quasi-static region), the deflection mode is global bending which matches well the deflection shape
382 expressed in Equation 1. Therefore the deflection shape of the laminated glass for damage level I can be
383 assumed to follow the global bending deformation, and the failure mode is flexural failure.
384 For damage level II (PVB rupture limit), this is observed from the numerical analysis when the
385 overpressure of the imposed blast loading is p=30 kPa (the impulse is maintained at i=10000 kPa·ms in this
386 case). The damage of glass initiates near the boundaries, then cracking develops all over the panel as a result
387 of bending deformation. By the time when PVB rupture occurs, the deformation resembles a rectangular
388 membrane case in a similar way as the damage level II in the impulsive region described in Section 3.1.2.
389 Therefore for damage level II in the quasi-static region the deflection function can be assumed to also follow
390 the membrane deflection.
391 As the overpressure further increases to reach damage level III, herein with p=50 kPa and i=10000
392 kPa·ms, the observed failure mode does not show much difference from that of damage level II. This is due
393 to the fact that the overpressure is not large enough to cause a local tensile failure at the early stage of the
394 response, and the PVB interlayer develops large tensile deformation resulting in tensile failure finally.
395 However, as the laminated glass fails at a marked speed for damage level III, the required overpressure is
396 larger than that for damage level II such that the remaining kinetic energy after PVB ruptures is able to

launch the debris. Therefore, the same deflection function can be adopted for laminated glass for damage level II and III in the quasi-static region.

4. ANALYTICAL APPROACH FOR CALCULATION OF ASYMPTOTES OF P-I DIAGRAMS

Based on the failure modes and the deflection functions established in Section 3, the impulse asymptotes and overpressure asymptotes for different damage levels can be formulated by means of the energy method. In this section, the solutions for the overpressure and the impulse asymptotes for the three different damage levels are presented.

For generality, the dimension of the laminated glass panel are assumed to be $a \times b \times (2h_g + h_i)$, where a and b are the length and width of the laminated glass panel respectively ($a \geq b$), and h_g and h_i represent the nominal thicknesses of the glass ply and the PVB interlayer respectively. The boundary condition for the laminated glass panel is assumed as fixed due to the constraint of the frame. The air blast load is assumed to act in the normal direction to the glass panel and uniformly distributed.

4.1 BASIC METHODOLOGY

Table 3 summarizes the relevant energy transformation for different loading types and damage levels. In order to calculate each part of the energy, the equivalent SDOF parameters of the laminated glass panel are firstly calculated, in which the displacement equivalence principle is adopted. Based on the assumed shape function $\psi^k(x,y)$, the equivalent mass M_e and load P_e of the laminated glass panel can be obtained as (Biggs 1964):

$$M_e^k = \iint m^*[\psi^k(x,y)]^2 dxdy \tag{3a}$$

$$P_e^k = \iint p\psi^k(x,y)dxdy \tag{3b}$$

where m^* is the equivalent mass per unit area of pre-crack laminated glass panel, which equals $2\rho_g h_g + \rho_i h_i$ (Wei and Dharani 2006). p is the overpressure acting on the glass panel and k represents different damage

levels. As mentioned in Section 3.1 and 3.2, under impulsive loading, the load duration is so short compared with the natural period of the laminated glass panel that the imposed blast load can be considered as a pure impulse *i*. From impulse-momentum transfer, an initial velocity $v_0^k = \frac{iab}{M_e^k}$ at the panel center can be obtained, where *iab* equals to the total impulse acting over the slab, and M_e is the equivalent mass (Equation 3a). Accordingly, the initial kinetic energy of the system can be found as $V_0^k = \frac{1}{2}\frac{(iab)^2}{M_e^k}$. In the quasi-static region, the applied pressure is considered to be constant, so the work done by the pressure is $W^k = P_e^k \cdot w_f^k$, where P_e^k is the equivalent load (Equation 3b), and w_f^k represents the final deflection at panel centre for different damage levels.

Based on the energy conservation principle and the governing failure mode discussed in Section 3, the external work done by blast loading will fully transform into internal strain energy in the laminated glass for damage level I and II since there is no residual kinetic energy. For damage level III, the external work will partly transform into the internal strain energy, and partly transform into residual kinetic energy. The residual kinetic energy can be calculated as $V_r = \frac{1}{2} M_e^{III} v_r^2$, in which v_r is the residual velocity at the panel centre that can be determined according to a specific design hazard level. Once the internal strain energy for different damage level is determined based on specified failure criteria, the imposed impulse or overpressure can be calculated based on energy conservation principle. It should be noted that there exists fracture energy due to glass cracking for damage level II and III. However, this part of energy is relatively small comparing to the internal strain energy in the cracked laminated glass at PVB rupture moment (Cormie et al. 2009), and it is even smaller in the total energy taking into account the residual kinetic energy for damage level III, so it is neglected. The determination of the internal energy in the laminated glass for different damage levels will be detailed in the following section.

4.1.1 Damage level I (Impulse region and quasi-static region)

According to the analysis in Section 3.1.1 and 3.2, the same deflection function expressed with Equation (1)

can be adopted for the glass crack limit in both quasi-static and impulse regions. Therefore the internal strain energy is the same for these two conditions.

In the pre-crack stage, the internal strain energy of the laminated glass is mainly the bending strain energy stored in the two glass plies. Based on the small-deflection theory of bending and the assumed deflection function, the stresses in the glass panel can be calculated using the stress-strain relations. By equating the maximum principal stress in the glass panel to the failure strength of glass σ_f, the failure displacement w_f can be obtained as:

$$w_f^I = \sigma_f \cdot \frac{1-v^2}{Eh\pi^2} \frac{a^2 b^2}{(a^2+vb^2)} \tag{4}$$

For pre-crack laminated glass panel, the equivalent properties for the whole panel can be written as: Young's modulus $E = \frac{E_g h_g + E_i h_i}{h_g + h_i}$, Poisson's ratio $v = \frac{v_g h_g + v_i h_i}{h_g + h_i}$ (Laura and Rossit 2001; Wei and Dharani 2006). Since the equivalent Young's modulus of the laminate is dominated by the glass stiffness, and meanwhile the governing mode for glass crack limit is global bending, which should not involve very high strain rate, the strain rate effect of the PVB would only have a small influence for the pre-crack stage analysis in current study. Therefore E_i is taken as a constant of 50MPa for dynamic modulus (corresponding to a strain rate of about $10s^{-1}$ (Zhang et al. 2015)) in the calculation for pre-crack stage to consider the strain rate effect implicitly. The other material parameters for glass and PVB are assumed to have the same values as listed in Table 1. At the onset of glass crack, the internal strain energy U_i^I can be obtained by:

$$U_i^I = \frac{1}{2} K_e^I w_f^{I^2} \tag{5}$$

where K_e^I is the equivalent stiffness and it can be obtained by:

$$K_e^I = \iint D^* \left\{ \left[\frac{\partial^2 \psi^I(x,y)}{\partial x^2} + \frac{\partial^2 \psi^I(x,y)}{\partial y^2} \right]^2 - 2(1-v) \left[\frac{\partial^2 \psi^I(x,y)}{\partial x^2} \frac{\partial^2 \psi^I(x,y)}{\partial y^2} - \frac{\partial^2 \psi^I(x,y)}{\partial x \partial y} \right] \right\} dxdy \tag{6}$$

in which D^* is the equivalent parameter of pre-crack laminated glass panel that equals to $\frac{2E_g}{3(1-v_g^2)}[h_g^2 + \frac{3h_i^2 h_g}{4} + \frac{3h_g^2 h_i}{2}] + \frac{2E_i h_i^3}{3(1-v_i^2)}$ (Wei and Dharani 2006), and $\psi^I(x,y)$ is the assumed deflection

function expressed by Equation (1).

4.1.2 Damage level II (Impulse region and quasi-static region)

For the PVB rupture limit, it may reasonably be assumed that glass has fully cracked and the membrane effect of PVB interlayer plays a dominant role in the post-crack response stage since the post-crack panel exhibits no bending stiffness. To understand the property of cracked laminated glass, high speed tensile tests have been carried out by Hooper et al. (2012). With the cracked laminated glass regarded as a homogeneous material, a post-crack model has been developed and the stress-strain relationships obtained from the tests are shown in Figure 13. In order to simplify the calculation, an equivalent linear elastic stress-strain relationship, as shown in Figure 14, is adopted based on the assumption of equivalent internal strain energy at the time of failure. The obtained equivalent modulus E_i^* can be used in the subsequent calculations.

According to the analysis in Section 3.1.2 and 3.2, the deflection function in Equation 2 is suitable for PVB rupture limit in both quasi-static and impulse regions. Therefore the internal strain energy is the same for these two conditions. Based on the membrane theory and the assumed deflection function (Equation 2), the total strain energy, which is only contributed by the tensile strain energy of cracked laminated glass, can be given by:

$$U_i = \frac{E_i^* h_i}{2(1-v_i^2)} \iint [\varepsilon_x^2 + \varepsilon_y^2 + 2v\varepsilon_x\varepsilon_y + \frac{1}{2}(1-v_i)\gamma_{xy}^2]dxdy \tag{7}$$

in which the strain components are given by:

$$\varepsilon_x = \frac{\partial \psi_2^{II}(x,y)}{\partial x} + \frac{1}{2}[\frac{\partial \psi_1^{II}(x,y)}{\partial x}]^2 \tag{8a}$$

$$\varepsilon_y = \frac{\partial \psi_3^{II}(x,y)}{\partial y} + \frac{1}{2}[\frac{\partial \psi_1^{II}(x,y)}{\partial y}]^2 \tag{8b}$$

$$\gamma_{xy} = \frac{\partial \psi_2^{II}(x,y)}{\partial y} + \frac{\partial \psi_3^{II}(x,y)}{\partial x} + \frac{\partial \psi_1^{II}(x,y)}{\partial x}\frac{\partial \psi_1^{II}(x,y)}{\partial y} \tag{8c}$$

485 According to the principle of minimum potential energy, the partial differential of the potential energy
486 function with respect to c_1 and c_2 (undetermined parameters in the Equation 2) should equal zero. Then the
487 relationship between c_1 and c_2 can be given by:

$$c_2 = \frac{29.58(a+b)[4(a^2+b^2)-3ab(1+v)]}{ab[88.74(a^2+b^2)(9-v)+128ab(1+v)]}c_1^2 \tag{9}$$

488 The maximum principal strain which occurs at the panel centre can be calculated by Equation (2) and
489 Equation (8), and the result is $\varepsilon_{\max} = \frac{2\pi c_2}{b}$. By equating the maximum principal strain $\varepsilon_{\max}$ to the failure
490 tensile strain of the cracked laminated glass ε_f (ε_f =0.2 is adopted in current study, obtained from uniaxial
491 Through-Cracked-Tensile test (Hooper et al. 2012)), the parameters c_1 and c_2 can be determined by Equation
492 (9) for PVB rupture limit. Consequently the total strain energy for PVB rupture limit U_i^{II} can be calculated
493 by Equation (7).
494
495 4.1.3 Damage level III (Quasi-static region)
496
497 Damage level III corresponds to the condition that the whole panel detaches from the supporting frame and
498 launches with a certain velocity v_r after PVB has ruptured. It should be noted that strictly speaking this
499 condition is not applicable for quasi-static region because in this region static equilibrium between the
500 external force and the internal resistance is presumed, so there will be no kinetic energy remaining.
501 Nevertheless, a fictitious overpressure asymptote for damage level III is proposed in this section for the
502 completion of the P-I curve. Since the same deflection function applies for damage level II and damage level
503 III in the quasi-static region, the internal energy for damage level III would be exactly the same as damage
504 level II.
505
506 4.2 DAMAGE LEVEL III IN IMPULSE REGION
507
508 As discussed in Section 3, damage level III in the impulse region involves local tensile failure mode in a

"belt" region along the boundary lines (Figure 10). The strain energy in this failure mode needs to be evaluated taking into consideration of the particular failure mode. In this section, a simplified PVB tension bar model is proposed for this purpose. The key parameter defining the model is the width of damage "belt" region D_s, and an empirical formula is derived to predict this parameter based on the numerical parametric results. The dependency of the ejection velocity on the failure mode is investigated numerically. Based on the numerical results, the critical ejection velocity defining the boundary between local tensile failure and the mixed failure is determined.

4.2.1 Simplified model for local tensile failure mode

The local tensile failure mode for the laminated glass may be simplified into a tension bar model as shown in Figure 15. Based on the numerical observations, after glass fracture, the glass in the clamped region (within the frame) remains intact and is able to transfer the tensile force in PVB to the frame. Therefore, a PVB tension bar is formed between the clamped end and the central "undeformed" region (Figure 10). The length of the tension bar equals to the width of damage belt region (D_s) while the total "width" of the tension bar equals to the perimeter of the belt (C),

$$C = 2\left[\left(a - 2D_s\right) + \left(b - 2D_s\right)\right] = 2(a + b - 4D_s) \tag{10}$$

The displacement, w_f, can be calculated through the geometric relationship (see Figure 15) as:

$$w_f^{III} = D_s \cdot \sqrt{[(\varepsilon_f + 1)^2 - 1]} \tag{11}$$

where ε_f is the failure strain of cracked laminated glass. Consequently the tensile stain energy of the cracked laminated glass throughout the damage "belt" zone can be obtained as:

$$U_i^{III} = Ch_i \sqrt{D_s^2 + w_f^{III^2}} E_i^* \varepsilon_f^2 \tag{12}$$

where E_i^* is the modulus of cracked laminated glass, which has been discussed in detail in Section 4.1.2.

To calculate the residual kinetic energy after overall detachment, the equivalent mass corresponding to the assumed deformation mode for damage level III is calculated using Equation (3a), and is given by

$$M_e^{III} = (2\rho_g h_g + \rho_i h_i)[ab - \frac{4}{3}(a+b)D_s + 2D_s^2] \quad (13)$$

Accordingly, the residual kinetic energy can be calculated as $V_r = \frac{1}{2} M_e^{III} v_r^2$, in which v_r is the ejection velocity of the core region of panel that may be assigned according to a specific design hazard level.

4.2.2 Determination of the width of damage belt zone (D_s)

To determine this parameter, a detailed parametric study is carried out to investigate the influence of various parameters, including the panel dimension, interlayer thickness, glass thickness and the velocity at which the broken laminated glass is ejected. The general setting of the FE model is the same as introduced in Section 2. The panel dimensions adopted in the parametric study basically cover the scope of practical applications. Based on the numerical results, empirical formula is proposed for the evaluation of the width of damage belt zone (D_s).

(a) Influence of panel dimension

Five representative dimensions are considered in the numerical parametric analysis, as listed in Table 4. The first three (labelled 1-1, 1-2 and 1-3) have the same area but with different aspect ratios, the remaining two (1-4 and 1-5) are in the same aspect ratio as case 1-1 but with different areas. All the specimens have the same thickness of 7.52mm (3+1.52+3mm) and the boundary condition is four-side fixed. The imposed loads are proportional to total panel mass so that the ejection velocity is kept the same.

For a rectangular panel, D_s is taken as the average of the belt zone widths in x- and y-directions D_{sa} and D_{sb}, which are determined by the horizontal length between boundary and the first point with the rotation angle smaller than 10° along the deflection profiles of central lines. As can be observed in Table 4, in fact the widths in both directions do not differ significantly, therefore it is reasonable to use an average value for D_s.

The variations of D_s for panels of different dimensions are shown in Table 4 and Figure 16. As can be

556 seen, the variations of D_s for different cases are basically within ±10%, indicating that D_s is insensitive to the
557 panel dimensions.
558
559 (b) Influence of the ratio of PVB interlayer thickness to glass thickness
560
561 Previous research has shown that PVB that bridges between glass cracks plays a very important role
562 in the post-crack behaviour of laminated glass, and the bridging effect is highly dependent on the stiffness
563 ratio between PVB interlayer and the glass.
564 For this analysis, 4 typical interlayer thicknesses, ranging from 0.38mm to 2.28mm, and 4 typical
565 glass thicknesses, ranging from 3mm to 12mm, are considered (Table 5). To simplify the comparison, a
566 uniform panel dimension of 1000mm × 800mm is employed. It is noted that, two pairs of cases, namely case
567 2-1 and case 3-3, and case 2-2 and case 3-1, are designed specifically to share the same h_i/h_g ratio, but the
568 absolute thickness of the PVB interlayer and the glass layers are different.
569 As can be seen from the results in Table 5 and Figure 17, D_s increases with the PVB thickness. This
570 is because the bridging effect of the PVB between glass fragments is reinforced with the increase of the PVB
571 thickness, especially in the damage zone where only the PVB interlayer offers resistance after glass cracks.
572 When the thickness of PVB interlayer increases, the stiffness proportion of PVB interlayer in total laminated
573 glazing increases, while that of glass layer decreases. The change of the relative stiffness makes glass layer
574 relatively more 'weak', and more glass will crack before PVB ruptures, leading to a further development of
575 damage zone near boundaries. As the damage zone expands, more PVB interlayer is involved in load
576 bearing, which also results in a larger bearing capacity. On the other hand, D_s tends to decrease as the glass
577 thickness increases, as shown in Table 5 and Figure 18. This is because the increase of the glass thickness
578 weakens the relative bridging effect of the PVB. Once the PVB in the damage zone fails, the stress transfer
579 between the boundaries and the remaining (central) part of the panel will be terminated, as a result the
580 damage zone cannot develop any further.
581 Based on the above discussion, the bridge effect of PVB interlayer on D_s can be related to the
582 thickness ratio h_i/h_g in the following empirical formula. The suitability of this parameter can also be proved

583 through comparison between case 2-1 and case 3-3. The panels of these two cases are different in both
584 interlayer thickness and glass thickness, but they share the same h_i/h_g ratio (0.0633). It can be seen that the
585 D_s values of the two cases are basically the same (variation=3.33%), suggesting that the function of PVB-
586 bridge is mainly affected by the stiffness ratio between PVB and glass, rather than by h_i or h_g separately. The
587 same phenomenon can be observed when comparing case 2-2 and case 3-1; with the same h_i/h_g ratio
588 (0.1267) and the variation is only 2.94%. Therefore, it is believed that the parameter h_i/h_g is more
589 representative in reflecting the change of D_s than individual h_i or h_g.
590
591 (c) Relationship to ejection velocity
592
593 Ejection velocity is another important factor that correlates with the width of damage zone, D_s. For this
594 examination, a laminated glass panel of 1000mm × 800mm × 7.52mm (3+1.52+3mm) is subjected to
595 different levels of blast loadings with different impulse values, as listed in Table 6. The achieved ejection
596 velocities of the detached panel for different loadings are also listed in Table 6 and shown in Figure 19. As
597 can be seen, D_s decreases as ejection velocity increases with increase of the load impulse. In fact the local
598 tensile failure mode becomes increasingly dominant as more impact energy is imposed, resulting in the
599 decrease in D_s.
600 Attention is drawn to the fact that the ratio of residual kinetic energy to the total energy at the onset
601 of PVB rupture, expressed as $\lambda=V_r/(U_i^{III}+V_r)$, increases with the imposed impulse, which in turn affects the
602 failure mode. As is shown in Figure 20, $\lambda=0$ (at i=377kPa·ms) represents the critical state of damage level II,
603 where the imposed blast energy fully transforms into the internal energy of cracked laminated glass and
604 therefore there is no residual kinetic energy. In this case, the failure mode is global tensile failure, as
605 discussed in Section 3.1.3. With increasing the imposed impulse to 650kPa·ms, the residual velocity of the
606 laminated panel at PVB rupture moment is about 25 m/s, and local PVB tensile failure can be observed from
607 FE analysis.
608 It can therefore be postulated that a true local tensile failure, for which the proposed PVB tensile bar
609 model is applicable, would be guaranteed only if λ is large enough, otherwise the failure mode could be a

combination of global tensile failure and local tensile failure. Based on the above parametric analysis on the influence of ejection velocity, a critical residual kinetic energy ratio λ_c=0.7 is suggested as the lower limit to ensure the occurrence of a local tensile failure mode for damage level III. The corresponding critical ejection velocity v_{rc} is given by:

$$v_{rc} = \sqrt{\frac{2U_i^{III}\lambda_c}{M_e^{III}(1-\lambda_c)}} \tag{14}$$

(d) Empirical formula for D_s

Based on the above analyses, D_s is mainly influenced by the ratio of interlayer thickness to glass thickness, h_i/h_g, and the ejection velocity, v_r. Through a regression analysis, the following empirical formula is proposed to predict D_s for any residual velocity v_r exceeding the critical residual velocity v_{rc}:

$$D_s = 0.20(\frac{h_i}{h_g}+0.70)e^{-0.019v_r}, v_r \geq v_{rc} \tag{15}$$

Figure 21 shows the results using the above formula as compared to the original FE results. A close match is observed. It should be noted that for an ejection speed below the critical ejection velocity given by Equation (14), a mixed mode of failure is expected and is discussed in the following sub-section.

4.2.3 Simplified method for mix failure mode

When the ejection velocity is relatively small, the failure mode is a mixed mode combining global tensile failure and local tensile failure. Due to the complexity of such a mixed failure mode, it is difficult to come up with a uniform deflection function. Therefore, a transition index ξ is introduced herein to describe the failure mode transition between global tensile failure and local tensile failure:

$$\xi = \frac{v_r}{v_{cr}}, 0 \leq v_r \leq v_{cr} \tag{16}$$

If the ejection speed is 0 (ξ=0), the condition falls to the PVB rupture limit, which is global tensile failure. The corresponding critical impulse i_{cr}^{II} can be determined according to Section 4.1.2. When the ejection velocity reaches the critical ejection velocity v_{cr} (ξ=1), local tensile failure dominates, and the corresponding critical impulse $i_{cr}^{III}(v_{cr})$ can be determined based on the simplified PVB tension bar model. The critical impulse corresponding to an ejection velocity between 0 and v_{cr} may be determined using a linear interpolation, which is given by

$$i_{cr}^{III}(v_r) = \xi[i_{cr}^{III}(v_{cr}) - i_{cr}^{II}],\ 0 \le v_r \le v_{cr} \tag{17}$$

Based on Equation (10) to (15)，the critical ejection velocity and corresponding critical impulse for damage level II can be calculated, which are 28.5m/s and 706.9kPa·ms for laminated glass panel of dimension 1000mm × 800mm × 7.52mm, respectively. Through an interpolation by Equation (17), the critical impulse corresponding to an ejection velocity between 0 and v_{cr} are determined. Figure 22 shows a comparison between FE analysis results and the predictions by Equation (17), good agreement is observed.

5. RESULTS OF P-I DIAGRAMS AND VALIDATION

In this section, the above proposed methodology for constructing P-I curves is implemented and validated through comparison against published experimental results and numerical results. A typical laminated glass panel with a dimension of 1500mm×1200m×7.52mm is chosen as an example, and for damage level III ejection velocities of 10, 30 and 50m/s are considered.

5.1 Generation of P-I diagrams

The P-I curve can be expressed is in a general form as follows (Shi et al. 2008; Zhang et al. 2013):

$$(p - p_{cr}^k)(i - i_{cr}^k) = \alpha(\frac{p_{cr}^k}{2} + \frac{i_{cr}^k}{2})^\beta \tag{18}$$

where i_{cr}^{k}, p_{cr}^{k} are the critical impulse and critical overpressure for a given damage level k, respectively; α and β are shape parameters which determine the shape of the curve in the dynamic zone between the impulse and quasi-static asymptotes.

The impulse and overpressure asymptotes of P-I curve for different damage levels can be obtained using the analytical approach described in Section 4. Glass is considered as a brittle elastic material, and the material properties and failure criteria are taken as the same as those adopted in the numerical model (Table 1). The material properties for cracked laminated glass have been introduced in section 4.1.2. The calculated impulse and overpressure asymptotes for different damage levels are summarized in Table 7.

For the dynamic zone of the P-I curves, the shape parameters (α and β) are determined through numerical analysis. Different combinations of pressure and impulse are applied in the numerical model to simulate the behaviour of laminated glass panel subjected to different blast loading. Thereafter, the corresponding behaviour, such as damage state of glass panel and ejection speed, is extracted through numerical post-processing, and the boundaries between the predefined damage levels are identified. Based on a regression analysis, the shape parameters of P-I curve under different damage levels can be obtained, and the fitted curves are shown with solid lines in Figure 23. The obtained shape parameters for different damage levels are listed in Table 7.

As can be seen in Table 7, α and β is around 1.6 and 1.5, respectively, and the variation of both parameters are within 10%. It is therefore believed that α and β are relatively insensitive to the change of damage level, which is consistent with previous observations (Shi et al. 2008; Zhang et al. 2013). Hence, in the present study, α and β are considered as constants by taking an average value of α and β from the above simulated cases respectively, i.e. α = 1.68 and β = 1.50. As shown in Figure 23, the P-I curves generated using constant α and β (represented by dotted line) also show good agreement with numerical results, which demonstrates the effectiveness of adopting constant shape parameters.

5.2 Verification of the analytical predictions

The experimental cases reported by Hooper et al. (2012) and Zhang et al. (2015) are adopted for validation.

The structural and loading parameters for these cases are listed in Table 8. As can be seen in Figure 24, due to the limitation of the tests, most of the obtained blast loads were in the dynamic region and below damage level II (PVB rupture). The threshold of this damage level obtained from test results are in good agreement with the P-I curves in the dynamic region as generated using the present approach. This demonstrates that the proposed dynamic region shape parameters are suitable for the prediction of the dynamic response of laminated glass panels.

Due to limited availability of physical experiments, additional FE analyses have been conducted in both impulse and quasi-static regions to further validate the theoretical results of the impulse asymptotes and overpressure asymptotes of the P-I curves for different damage levels.

A series of numerical test points are set around the impulse and overpressure asymptotes obtained by the proposed theoretical method. The damage states of the laminated glass from the numerical simulations were extracted and classified into different damage levels. The asymptotes based on numerical results are determined by taking the average between the two close points that corresponds to different damage levels in the impulse region and the quasi-static region, respectively.

As can be seen from Figure 25 and Table 9, the results from the numerical simulation are generally in good agreement with the P-I curves generated using the proposed method, with differences mostly within 15%. The largest discrepancy exists with the impulse asymptote for damage level I. The impulse asymptote is 28 kPa·ms from the numerical result and it is 24.3kPa·ms from the theoretical prediction, yielding a difference of -15.36%. It can be explained that the boundary condition is assumed to be totally fixed in the theoretical model, whereas in the numerical model the glass panel is supported by a steel frame with cushion layers. With the assumption of a fixed boundary, the theoretical method gives an upper bound condition in terms of the stiffness of the boundaries, which will result in an overestimate of the internal stress and therefore an underestimate of the bearing capacity of the panel.

Further comparison is made between the current method and the P–I diagrams developed by other researchers, as shown in Figure 26. Hooper et al. (2012) has proposed P-I curves for the glass windows of dimension 1500mm×1200m×7.52mm (3+1.52+3mm) through numerical calculations. These curves match well with the present theoretical results for damage level I and damage level II. Zhang et al. (2013) proposed

an empirical formulae for predicting the impulse asymptote and overpressure asymptote for damage level II (PVB rupture limit) through numerical calculations and suggested shape parameters $\alpha = 2.4$ and $\beta = 1.2$. The generated curve matches well with the current study.

Summarising the above comparisons, the analytical method proposed in the present study is shown to be capable of producing satisfactory predictions covering comprehensively the impulse and overpressure asymptotes for different damage levels.

6. CONCLUSIONS

In this paper, a methodology for generating P-I diagrams is developed for framed PVB-laminated glass panel considering 3 typical damage levels, namely a) glass crack limit, b) PVB rupture limit and c) the panel detaching with a specified velocity. The overpressure asymptote and the impulse asymptote are derived analytically based on energy method, whereas the segment of the curve in dynamic region is established using an empirical approach based on numerical simulation results.

The deflection functions required in the producing of the P-I diagrams have been established according to the governing failure modes of the laminated glass panel subjected to different blast loading identified from numerical simulations. It is found that for the glass crack limit and PVB rupture limit, global deformation mode (bending or membrane) is dominant in both impulse and quasi-static regions. Local tensile failure mode is dominant for Damage level III in impulse region. A simplified PVB tensile bar model is proposed to describe this punching-type failure and an empirical formula for determining the damage region width D_s is derived based on numerical parametric study.

The P-I curves generated using the proposed approach are validated against published experiment results and further finite element simulations for different damage levels. The proposed method can be applied for different glass panel dimensions and therefore provide a means for quick estimation of the damage state and prediction of invading distance. It can also be extended for other types of interlayers.

ACKNOWLEDGEMENTS

The authors gratefully acknowledge the financial support by the National Natural Science Foundation of China under the grant No. 51678448 and the State Key Laboratory of Disaster Reduction in Civil Engineering, Tongji University under the grant No. SLDRCE 14-B-13.

REFERENCES

ASTM-E1300 (2012). Standard practice for determining load resistance of glass in buildings.

ASTM-F2248 (2012). Standard practice for specifying an equivalent 3-second duration design loading for blast resistant glazing fabricated with laminated glass.

Baker, W. E. (1983). Explosion hazards and evaluation, Elsevier Scientific Pub. Co.

Bennison, S. J., Sloan, J. G., Kristunas, D. F., Buehler, P. J., Amos, T. and Smith, C. A. (2005). "Laminated glass for blast mitigation: Role of interlayer properties." *Proceedings of Glass Processing Days, Tampere, Finland*.

Biggs, J. M. (1964). Introduction to structural dynamics.

BS EN 13541 (2012). Glass in building - Security glazing - Testing and classification of resistance against explosion pressure.

Chen, S., Wu, X. and Shu, W. (2015). The mechanical behaviour of polyvinyl butyral at intermediate strain rates. 3rd International Conference on Protective Structures (ICPS3). Newcastle, Australia.

Chen, S., Zhu, C. G., Li, G. Q. and Lu, Y. (2016). "Blast test and numerical simulation of point-supported glazing." *Advances in Structural Engineering*.

Cormie, D., Mays, G. C. and Smith, P. D. (2009). Blast effects on buildings, second ed. England Thomas Telford Publications.

Ge, J., Li, G.Q. and Chen, S.W. (2012). "Theoretical and experimental investigation on fragment behavior of architectural glass panel under blast loading." *Engineering Failure Analysis* **26**(12): 293–303.

GSA-TS01 (2003). Standard test method for glazing and window systems subject to dynamic overpressure loadings.

Hetherington, J. and Smith, P. (1994). "Blast and ballistic loading of structures." *Crc Press*.

Hidallana-Gamage, H. D., Thambiratnam, D. P. and Perera, N. J. (2014). "Numerical modelling and analysis of the blast performance of laminated glass panels and the influence of material parameters." *Engineering Failure Analysis* **45**(8): 65-84.

Hidallana-Gamage, H. D., Thambiratnam, D. P. and Perera, N. J. (2017). "Influence of the negative phase and support flexibility on the blast response of laminated glass panels." *Construction and Building Materials* **154** 462–481.

Hooper, P. A., Sukhram, R. A. M., Blackman, B. R. K. and Dear, J. P. (2012). "On the blast resistance of laminated glass." *International Journal of Solids & Structures* **49**(6): 899-918.

ISO 16933 (2007). Glass in building - Explosion-resistant security glazing - Test and classification for arena air-blast loading.

ISO 16934 (2007). Glass in building - Explosion-resistant security glazing - Test and classification by shock-tube loading.

Iwasaki, R., Sato, C., Latailladeand, J. L. and Viot, P. (2007). "Experimental study on the interface fracture toughness of PVB (polyvinyl butyral)/glass at high strain rates." *International Journal of Crashworthiness* **12**(3): 293-298.

Jarrett D.E. (1968). "Derivation of the british explosives safety distances." *Annals of the New York Academy of Sciences* **152**(1): 18-35.

Krauthammer, T. and Altenberg, A. (2000). "Negative phase blast effects on glass panels." *International Journal of Impact Engineering* **24**(1): 1-17.

Larcher, M., Arrigoni, M., Bedon, C., Doormaal, A. V., Haberacker, C., Hüsken, G., Millon, O., Saarenheimo, A., Solomos, G. and Thamie, L. (2016). "Design of blast-loaded glazing windows and façades: a review of essential requirements towards standardization." *Advances in Civil Engineering,2016,(2016-8-7)* **2016**: 14 pages.

Larcher, M., Solomos, G., Casadei, F. and Gebbeken, N. (2012). "Experimental and numerical investigations of laminated glass subjected to blast loading." *International Journal of Impact Engineering* **39**(1): 42-50.

Laura, P. A. A. and Rossit, C. A. (2001). "The Behavior of Sandwich Structures of Isotropic and Composite Materials : by Jack R. Vinson; 1999, TECHNOMIC Publishing Company, Inc., Lancaster, PA, USA, 378 pp." *Ocean Engineering* **28**(10): 1437-1438.

Li, Q. M. and Meng, H. (2002). "Pressure-Impulse Diagram for Blast Loads Based on Dimensional Analysis and Single-Degree-of-Freedom Model." *Journal of Engineering Mechanics* **128**(1): 87-92.

LS-DYNA Keyword user's manual (2007). Livermore Software Technology Corporation.

Merrifield R. (1993). "Simplified calculations of blast induced injuries and damage." *Report no. 37, Health and Safety Executive Specialist Inspector*.

Nawar, M., Salim, H., Lusk, B. and Kiger, S. (2015). "Modeling and Shock Tube Testing of Architectural Glazing Systems for Blast Resistance." *Journal of Structural Engineering* **141**(7): 04014174.

Norville, H. S., Harvill, N. C., Edward, J., Shariat, S. and Mallonee, S. (1999). "Glass-Related Injuries in Oklahoma City Bombing." *Journal of Performance of Constructed Facilities* **13**(2): 50-56.

Pelfrene, J., Kuntsche, J., Dam, S. V., Paepegem, W. V. and Schneider, J. (2016). "Critical assessment of the post-breakage performance of blast loaded laminated glazing: experiments and simulations." *International Journal of Impact Engineering* **88**.

Shi, Y., Hao, H. and Li, Z. X. (2008). "Numerical derivation of pressure–impulse diagrams for prediction of RC column damage to blast loads." *International Journal of Impact Engineering* **35**(11): 1213-1227.

Spiller, K., Packer, J. A., Seica, M. V. and Yankelevsky, D. Z. (2016). "Prediction of annealed glass window response to blast loading." *International Journal of Impact Engineering* **88**: 189-200.

Teich, M. and Gebbeken, N. (2010). "The Influence of the Underpressure Phase on the Dynamic Response of Structures Subjected to Blast Loads." *International Journal of Protective Structures* **1**(2): 219-234.

Timmel, M., Kolling, S., Osterrieder, P. and Bois, P. A. D. (2007). "A finite element model for impact simulation with laminated glass." *International Journal of Impact Engineering* **34**(8): 1465-1478.

Timoshenko, S. P. (1940). "Theory of plates and shells." *Studies in Mathematics & Its Applications Elsevier Amsterdam* **6**(3760): 606.

UFC 4-010-01 (2013). "DoD Minimum Antiterrorism Standards for Buildings."

Weggel, D. C. and Zapata, B. J. (2008). "Laminated Glass Curtain Walls and Laminated Glass Lites Subjected to Low-Level Blast Loading." *Journal of Structural Engineering* **134**(3): 466-477.

Weggel, D. C., Zapata, B. J. and Kiefer, M. J. (2013). "Properties and Dynamic Behavior of Glass Curtain Walls with Split Screw Spline Mullions." *Journal of Structural Engineering* **133**(10): 1415-1425.

Wei, J. and Dharani, L. R. (2005). "Fracture mechanics of laminated glass subjected to blast loading." *Theoretical & Applied Fracture Mechanics* **44**(2): 157-167.

Wei, J. and Dharani, L. R. (2006). "Response of laminated architectural glazing subjected to blast loading." *International Journal of Impact Engineering* **32**(12): 2032-2047.

Zhang, X., Hao, H. and Ma, G. (2013). "Parametric study of laminated glass window response to blast loads." *Engineering Structures* **56**(6): 1707-1717.

Zhang, X., Hao, H., Shi, Y. and Cui, J. (2015). "The mechanical properties of Polyvinyl Butyral (PVB) at high strain rates." *Construction & Building Materials* **93**: 404-415.

Zhang, X., Zou, Y., Hao, H., Li, X., Ma, G. and Liu, K. (2012). "Laboratory Test on Dynamic Material Properties of Annealed Float Glass." *International Journal of Protective Structures* **3**(4): 407-430.

Zhang, X. H., Hao, H. and Ma, G. W. (2013). "Parametric study of laminated glass window response to blast loads." *Engineering Structures* **56**(6): 1707-1717.

Zhang, X. H., Hao, H. and Wang, Z.Q. (2015). "Experimental study of laminated glass window responses under impulsive and blast loading." *International Journal of Impact Engineering* **78**: 1-19.

Table 1: Material properties adopted in the finite element model

Material	Density (kg/m^3)	Elastic modulus (N/m^2)	Poisson's ratio	Material model	Material No. in Ls-dyna	Failure criterion
Float glass	2.56e3	7.2e10	0.22	Elastic	Mat_001	First principle stress=80MPa
PVB	1.1e3	Rate dependent	0.495	Rate dependant plasticity	Mat_019	First principle strain=1.2
Steel frame	7.86e3	2.1e11	0.288	Plastic kinematic	Mat_003	——
Silicon cushion	1e3	3.5e6	0.495	Elastic	Mat_001	First principle strain=1.6

Note: "—"represents no failure criterion is defined.

Table 2: Blast loadings from the tests (Hooper et al. 2012)

Test No.	Equivalent TNT charge (kg)	Standoff distance (m)	Reflected pressure (kPa)	Reflected impulse (kPa·ms)
1	15	13	140	284
2	15	10	180	391

Table 3. Energy transformation relationships for different loading types and damage levels

<table>
<tr><th>Loading type</th><th>Damage level</th><th colspan="4">Energy composition</th></tr>
<tr><td rowspan="3">Impulsive loading</td><td>I</td><td rowspan="3">Initial kinetic energy V_0^k</td><td rowspan="6"></td><td colspan="2">Strain energy of glass plies U_i^I</td></tr>
<tr><td>II</td><td colspan="2">Strain energy of cracked laminated glass U_i^{II}</td></tr>
<tr><td>III</td><td>Strain energy of cracked laminated glass U_i^{III}</td><td>Residual kinetic energy V_r</td></tr>
<tr><td rowspan="3">Quasi-static loading</td><td>I</td><td rowspan="3">Work done by the pressure W^k</td><td colspan="2">Strain energy of glass plies U_i^I</td></tr>
<tr><td>II</td><td colspan="2">Strain energy of cracked laminated glass U_i^{II}</td></tr>
<tr><td>III</td><td>Strain energy of cracked laminated glass U_i^{III}</td><td>Residual kinetic energy V_r</td></tr>
</table>

Note: *k* represents the corresponding levels, which equals I, II or III.

Table 4. Effect of panel dimension on the width of damage zone (D_s)

Numerical test No.	a (m)	b (m)	a/b	h_g (mm)	h_i (mm)	Ejection velocity (m/s)	D_{sa} (m)	D_{sb} (m)	Average D_s (m)
1-1	1.0	0.8	1.25	2×3	1.52	35.81	0.1000	0.0875	0.0938
1-2	1.2	0.675	1.78			36.42	0.1050	0.1050	0.1050
1-3	1.6	0.5	3.2			35.03	0.1050	0.0900	0.0975
1-4	2.0	1.6	1.25			35.62	0.0900	0.0900	0.0900
1-5	3.0	2.4	1.25			35.80	0.0900	0.1050	0.0975

Table 5. Effect of PVB interlayer thickness and glass thickness on the width of damage zone (D_s)

Numerical test No.	a (m)	b (m)	h_g (mm)	h_i (mm)	h_i/h_g	Ejection velocity (m/s)	D_{sa} (m)	D_{sb} (m)	Average D_s (m)
2-1	1.0	0.8	2×3	0.38	0.0633	36.07	0.0800	0.0700	0.0750
2-2				0.76	0.1267	34.05	0.0800	0.0900	0.0850
2-3				1.52	0.2533	35.81	0.1000	0.0875	0.0938
2-4				2.28	0.3800	36.21	0.1200	0.1050	0.1125
3-1			2×6	1.52	0.1267	36.64	0.0900	0.0850	0.0875
3-2			2×8		0.0950	36.04	0.0800	0.0700	0.0750
3-3			2×12		0.0633	35.72	0.0750	0.0700	0.0725

Table 6. Effect of ejection velocity on the width of damage zone (D_s)

Numerical test No.	a (m)	b (m)	h_g (mm)	h_i (mm)	i (kPa·ms)	Ejection velocity (m/s)	D_{sa} (m)	D_{sb} (m)	Average D_s (m)
4-1	1.0	0.8	2×3	1.52	800	35.81	0.1000	0.0875	0.0938
4-2					600	15.12	0.1800	0.1500	0.1650
4-3					1000	57.65	0.0600	0.0600	0.0600
4-4					1200	78.24	0.0500	0.0450	0.0475
4-5					600	15.12	—	—	—
4-6					500	11.47	—	—	—
4-7					450	5.94	—	—	—
4-8					400	2.04	—	—	—

Note：“—”represents mix failure occurs instead of significant punching failure, so that damage zone cannot be identified.

Table 7: Parameters for generating P-I curves

Damage level	Analytical result		α	β
	P_{cr} (kPa)	i_{cr} (kPa·ms)		
I	8.01	24.26	1.67	1.44
II	26.50	442.83	1.62	1.51
III_a (v_r=10m/s)	41.25	530.14	1.66	1.49
III_b (v_r=30m/s)	62.27	692.62	1.73	1.52
III_c (v_r=50m/s)	89.06	878.84	1.64	1.48
Average value			1.68	1.50

Table 8: Blast loadings from published experimental results

Size (m^2)	Thickness (mm)	TNT charge (kg)	Standoff distance (m)	Scaled distance (m/kg^1/3)	Reflected overpressure (kPa)	Reflected impulse (kPa·ms)
1.5×1.2	3+1.52+3	10	10	4.64	121.1	395
		10	9	4.18	168.6	476.1
		10	12.3	5.71	82.2	413.3
		15	10	4.05	180	391
		30	14	4.51	132	413

Table 9: Comparison between the asymptotes obtained from analytical results and FEA results

Damage level	FEA result		Analytical result	
	P_{cr} (kPa)	i_{cr} (kPa·ms)	P_{cr} (kPa)	i_{cr} (kPa·ms)
I	9	28	8.01 (-11.11%)	24.26 (-15.36%)
II	28	400	26.50 (-5.36%)	442.83 (10.71%)
III_a (v_r=10m/s)	45	550	41.25 (-9.09%)	530.14 (-3.6%)
III_b (v_r=30m/s)	70	650	62.27 (-11.04%)	692.62 (6.46%)
III_c (v_r=50m/s)	80	800	89.06 (11.33%)	878.84 (9.86%)

Note: Values in parentheses are corresponding error between simplified analytical model predictions and FEA results.

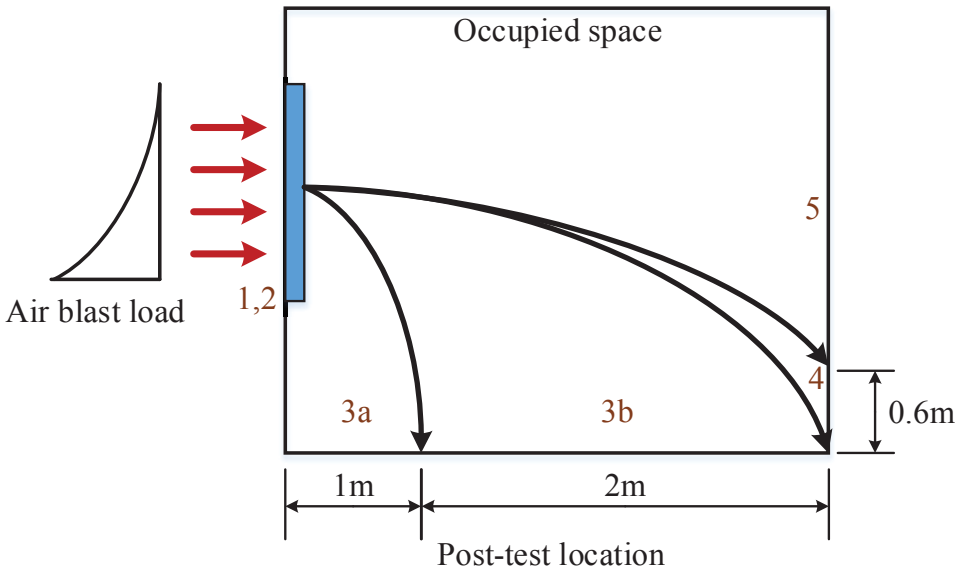

Figure 1: Performance conditions for window system response in GSA/ISC (2003)

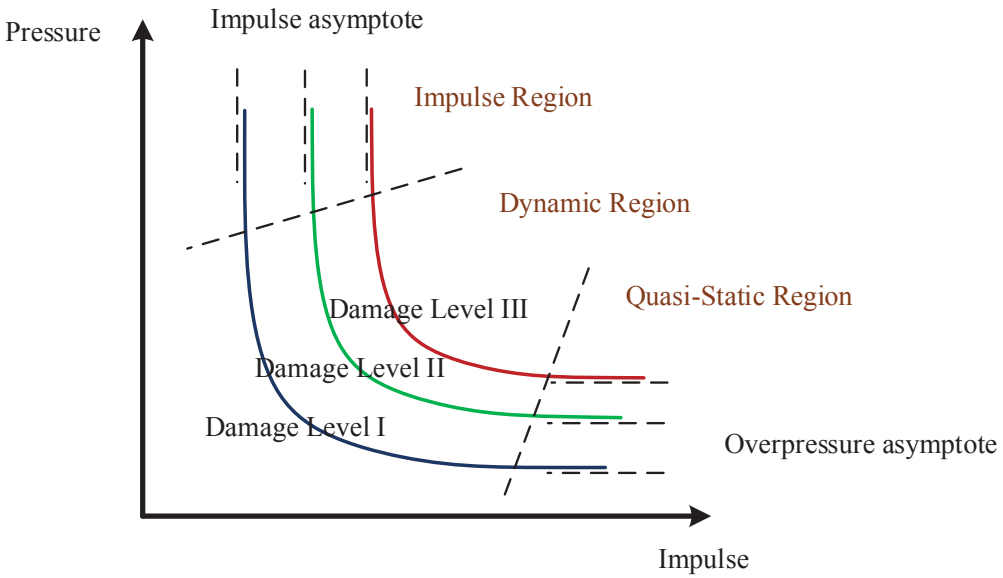

Figure 2. Characteristics of P-I curves for different damage levels

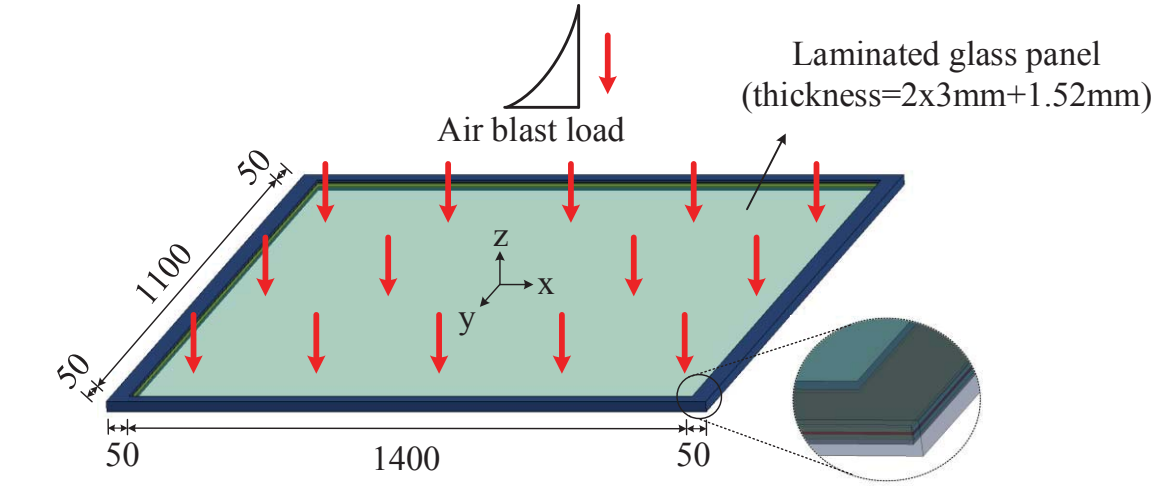

a. Geometry

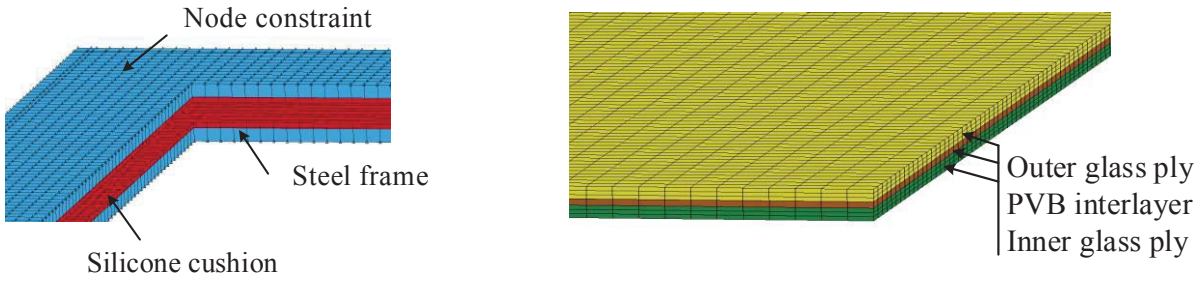

b. Element meshing

Figure 3. Finite element model

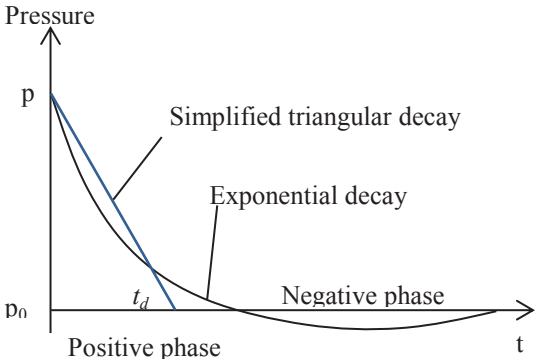

Figure 4. Simplified blast load

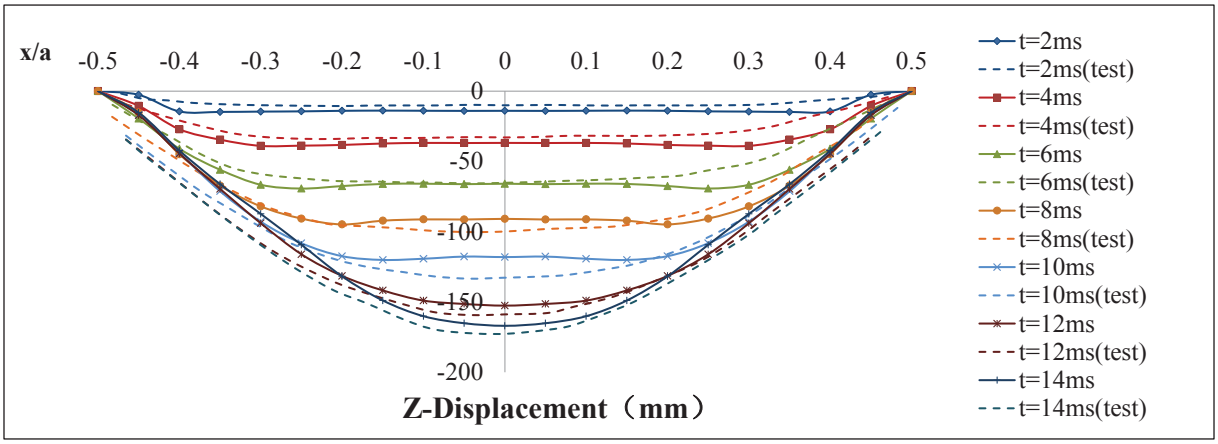

a. 15kg TNT @13 m

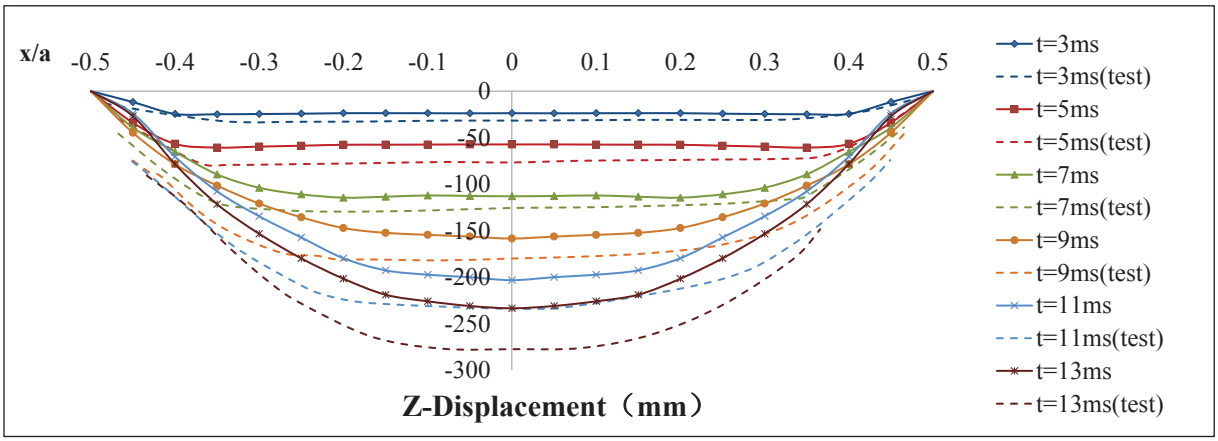

b. 15kg TNT @10 m

Figure 5. Validation of FE model against Hooper's test (Hooper et al. 2012)

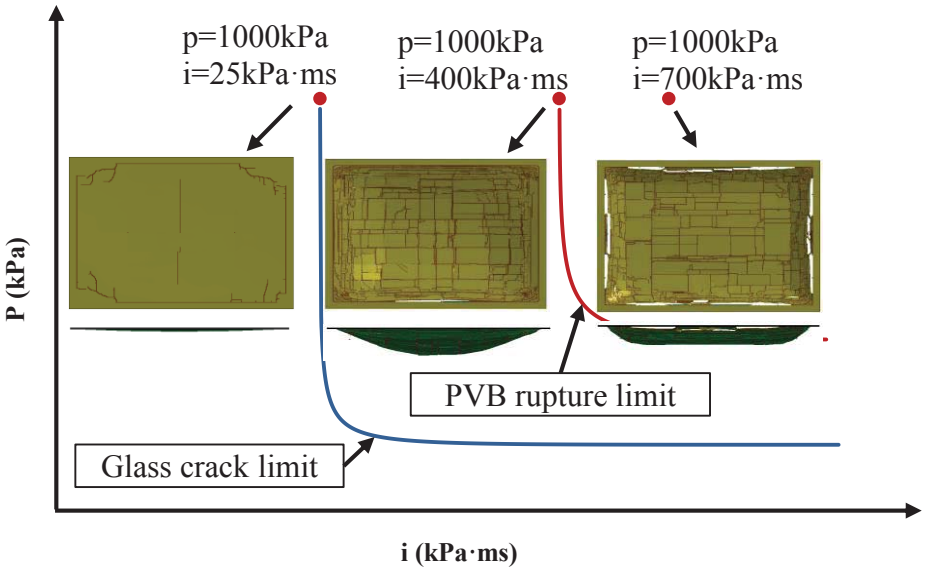

Figure 6. Failure modes of glass panels subjected to different impulsive loadings

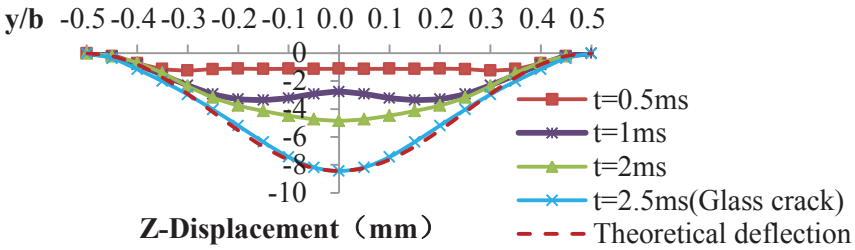

Figure 7. Deflection profiles along window central line under impulsive loading for damage level I, based on FE simulation

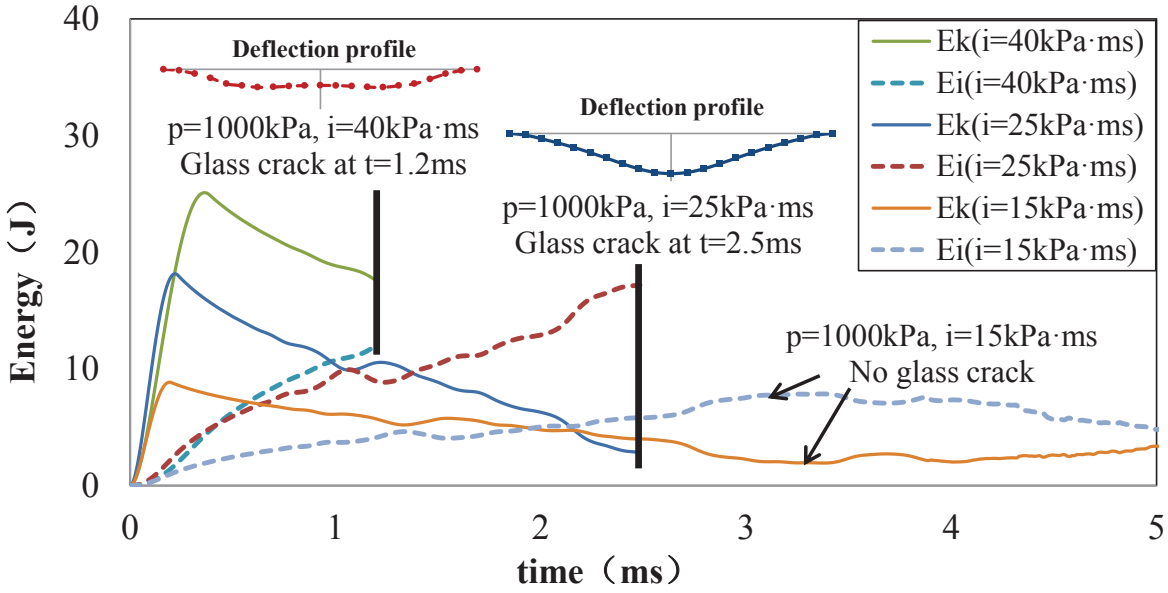

Figure 8. Typical kinetic energy and internal energy time histories

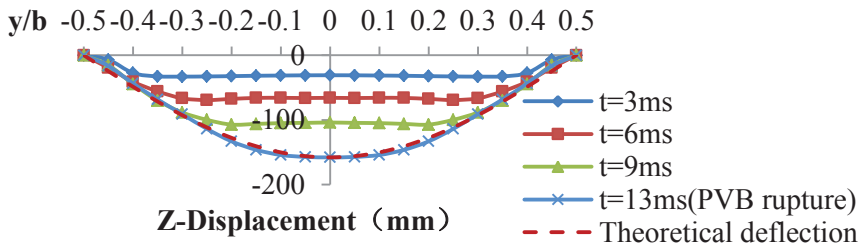

a. Out-of-plane deflection

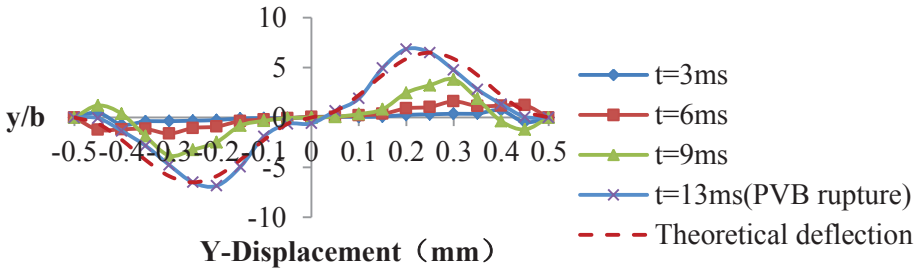

b. In-plane deflection

Figure 9. Deflection profiles at the window central line under impulsive loading for damage level II, based on FE simulation

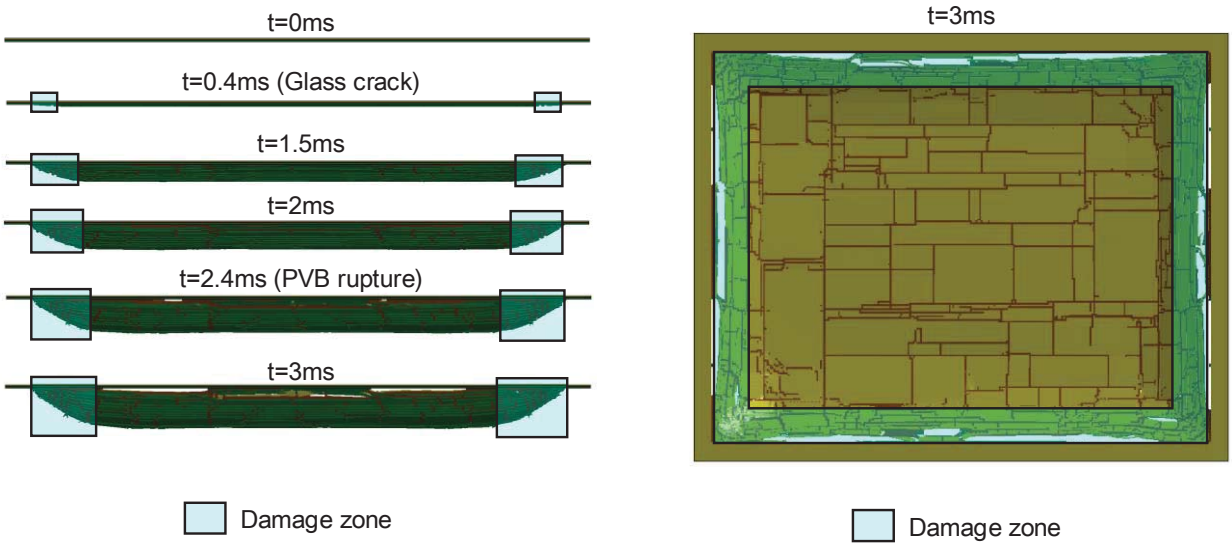

a. Side view

b. Front view (at t=3ms)

Figure 10. Deflection mode along panel central line from FE simulation (p=1000kPa, i=700kPa·ms)

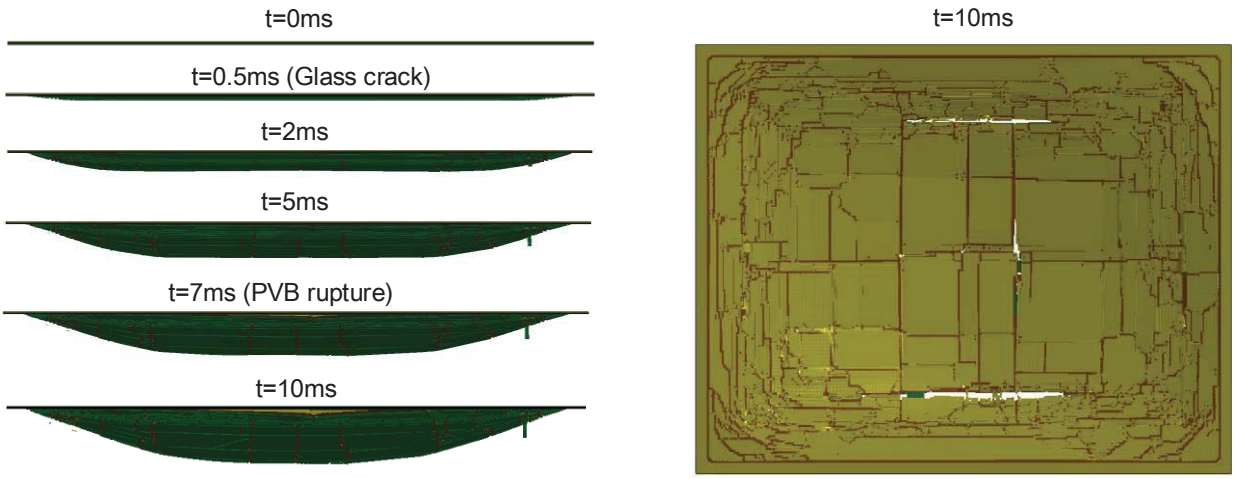

a. Side view

b. Front view (at t=10ms)

Figure 11. Deflection mode at the window central line from FEA (p=1000kPa, i=550kPa·ms), based on FE simulation

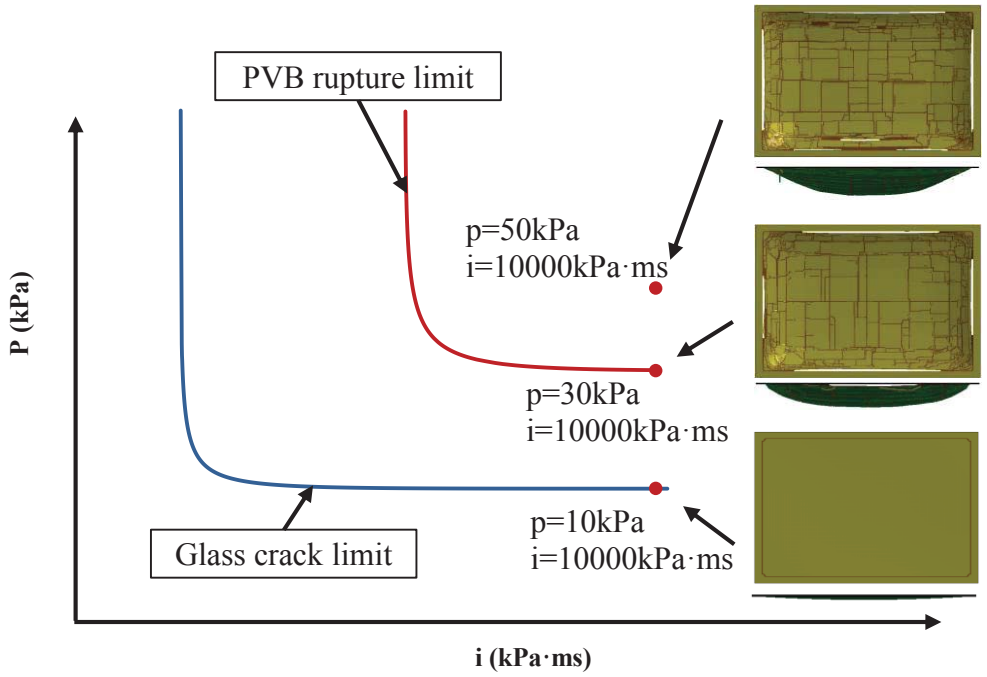

Figure 12. Failure mode of glass panels subjected to different quasi-static loadings

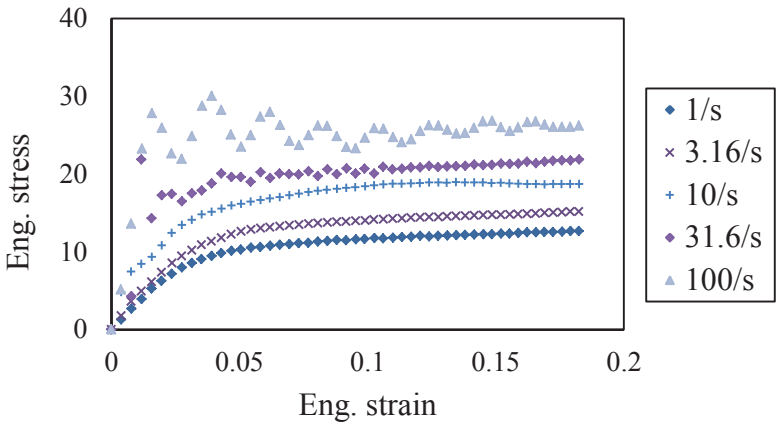

Figure 13. Tensile stress-strain relationship of 7.52 mm cracked laminated glass (Hooper et al. 2012)

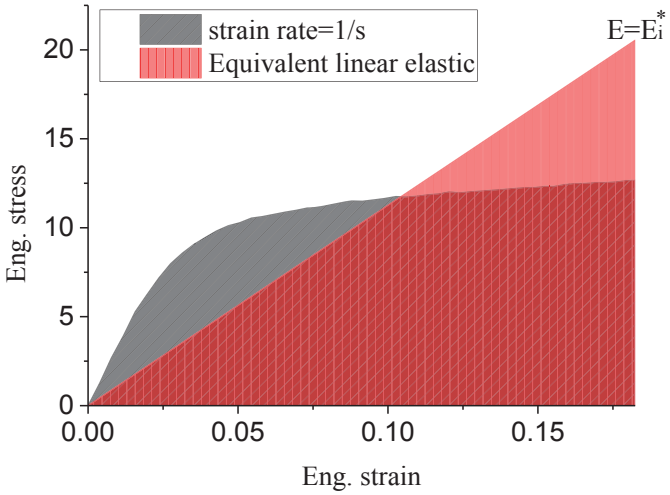

Figure 14. Simplified linear elastic stress-strain relationship of 7.52 mm cracked laminated glass

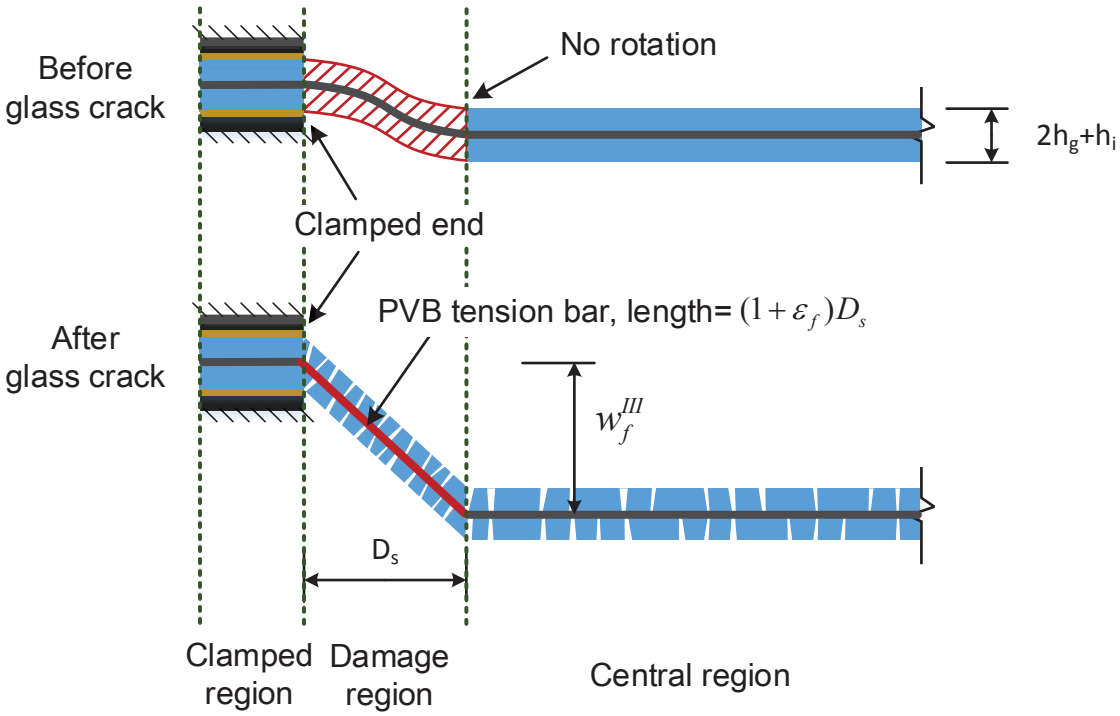

Figure 15. Simplified PVB tension bar model

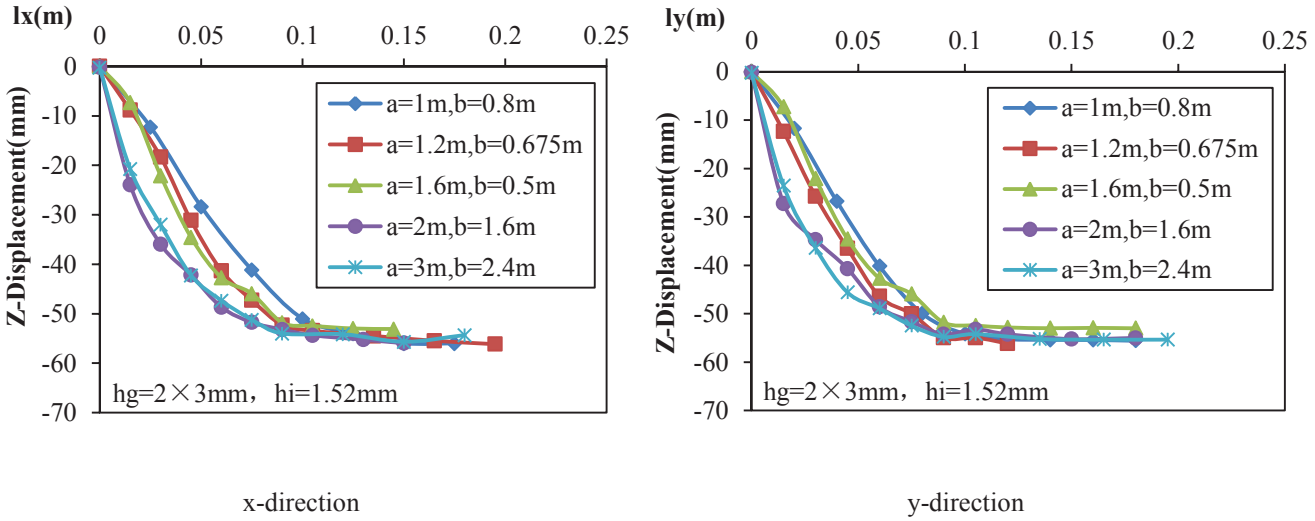

x-direction

y-direction

Figure 16. Deflection profiles along panel central line for different dimensions under impulsive loading

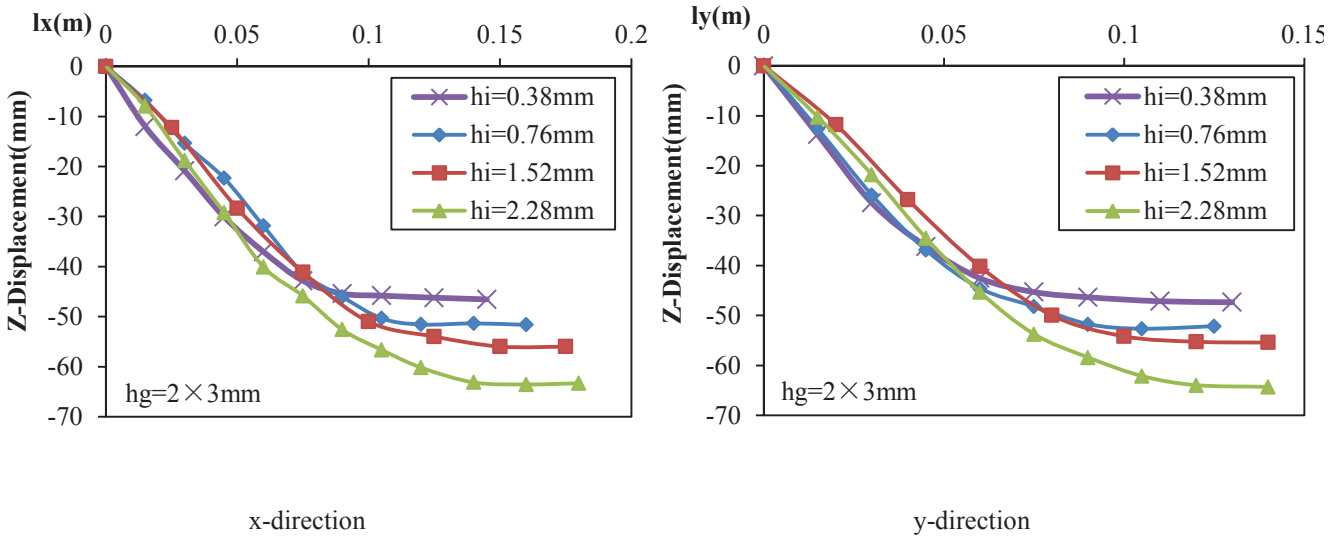

x-direction

y-direction

Figure 17. Deflection profiles along panel central line for different PVB interlayer thicknesses under impulsive loading

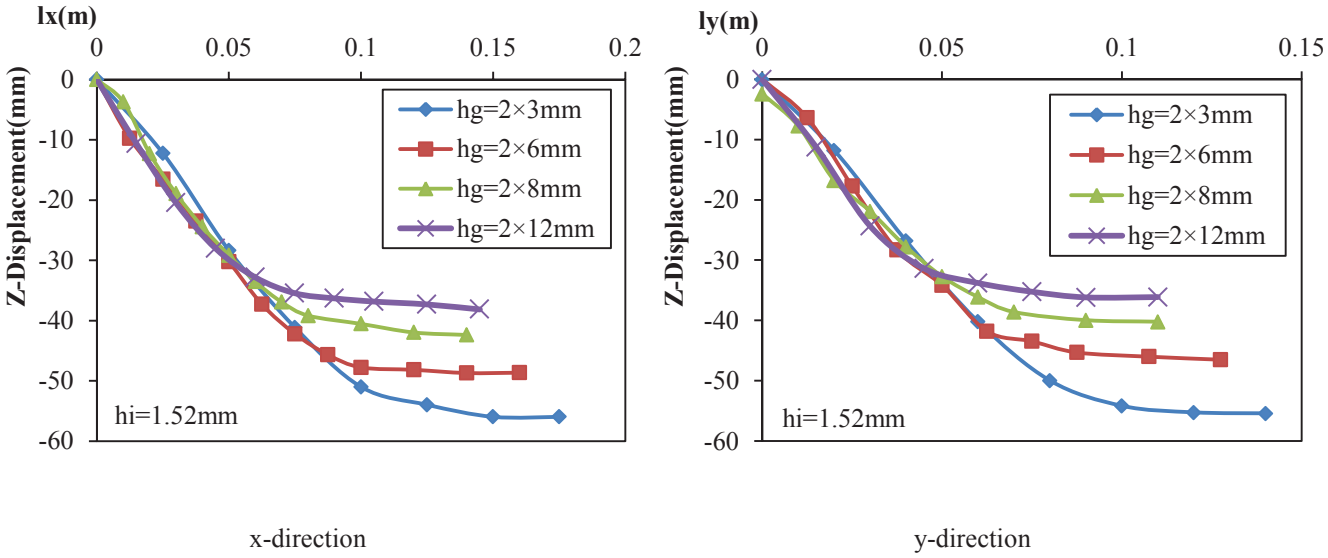

x-direction

y-direction

Figure 18. Deflection profiles along panel central line for different glass thicknesses under impulsive loading

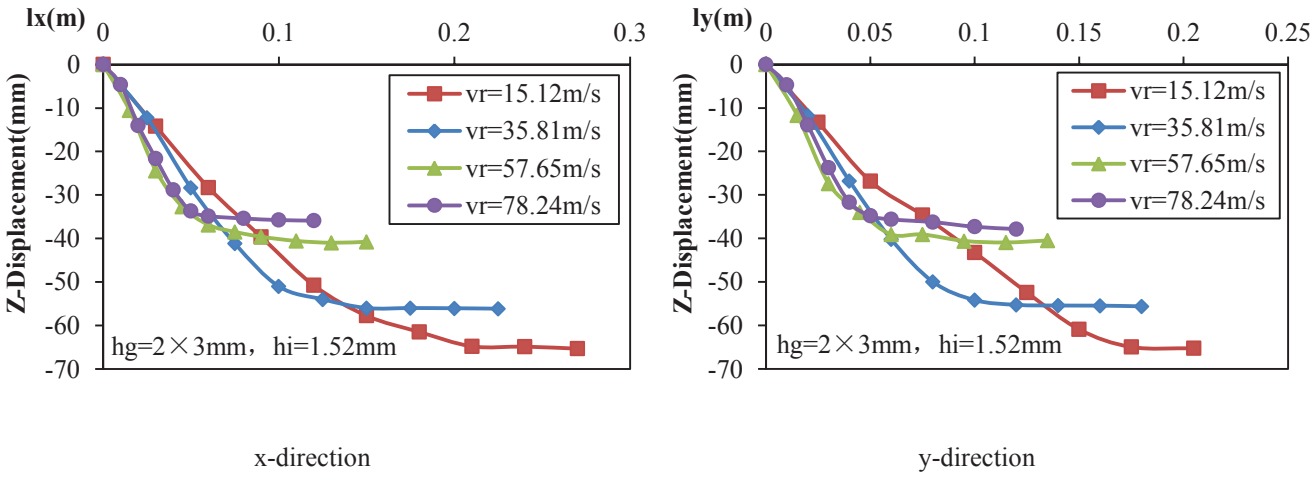

x-direction

y-direction

Figure 19. Deflection profiles along panel central line for different ejection velocities under impulsive loading

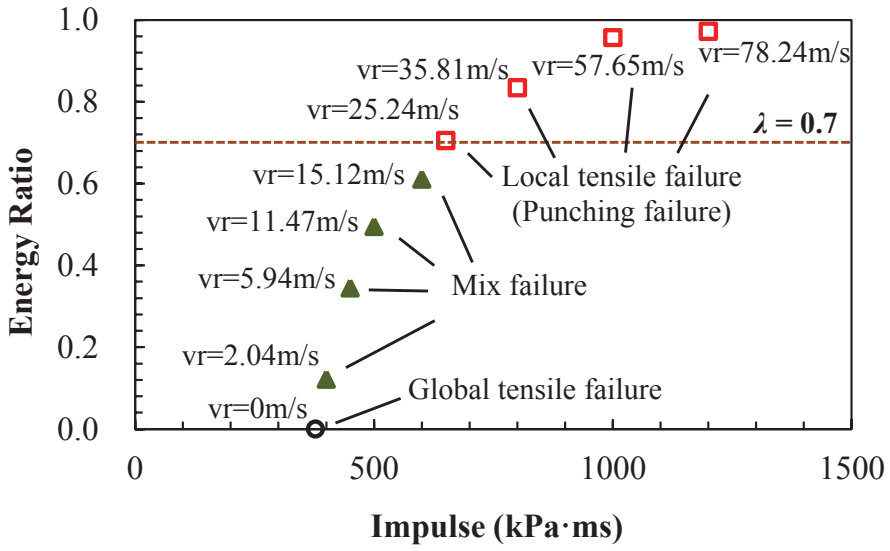

Figure 20: Relationship between energy ratio and imparted impulse

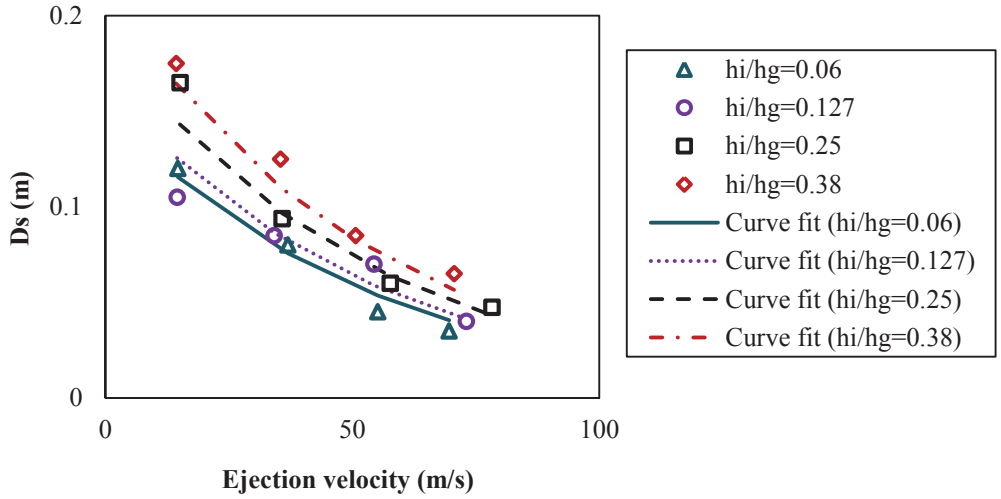

Figure 21: Comparison of D_s from numerical results and empirical formula predictions

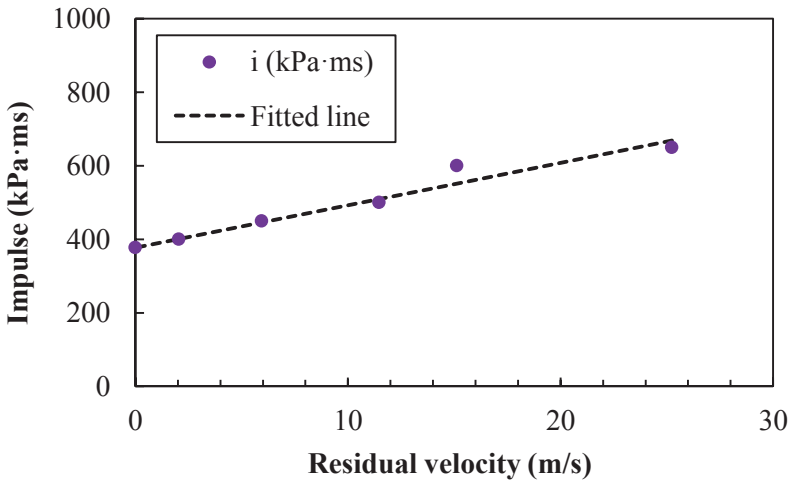

Figure 22: Critical impulse values corresponding to ejection velocities below v_{rc}

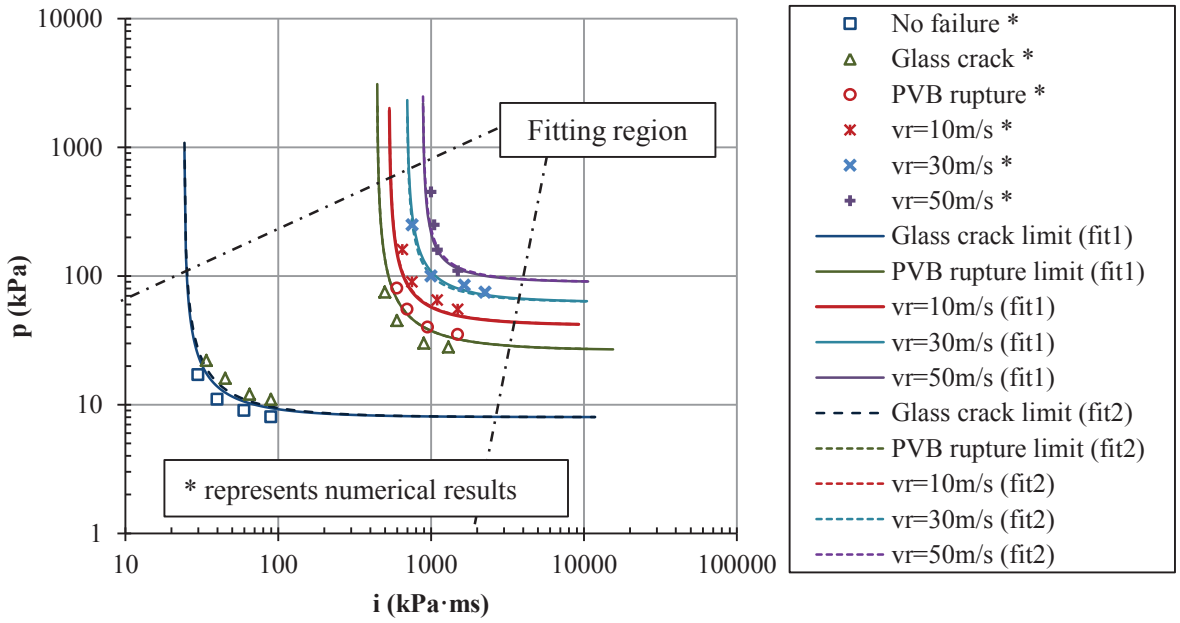

Figure 23. Comparison between the generated P-I curves and FEA results in dynamic region

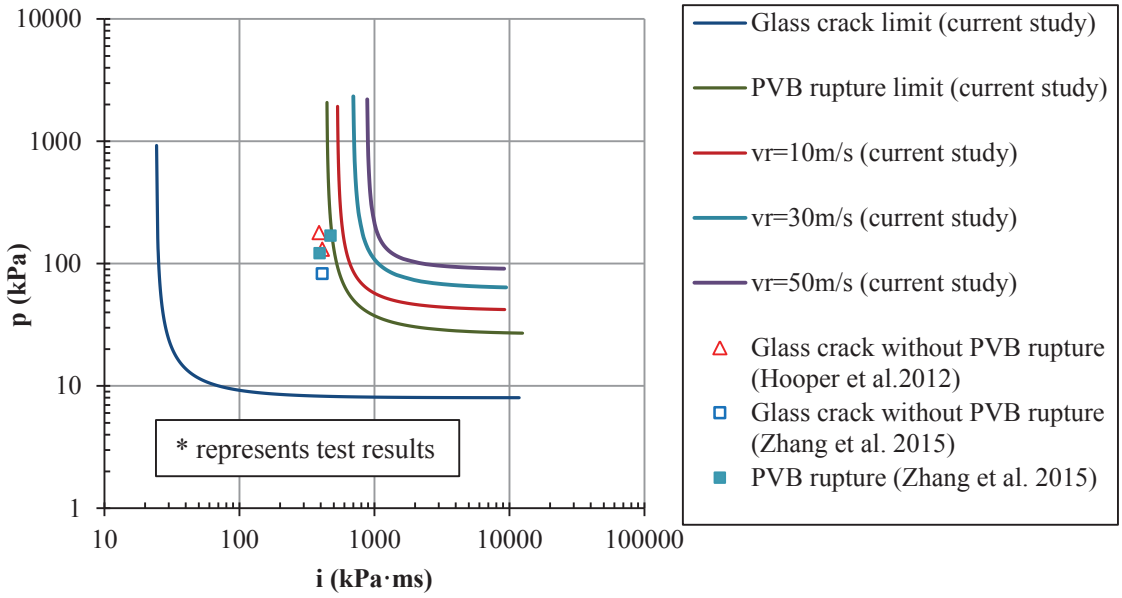

Figure 24. Comparison between proposed P-I diagrams with experimental results from other researchers

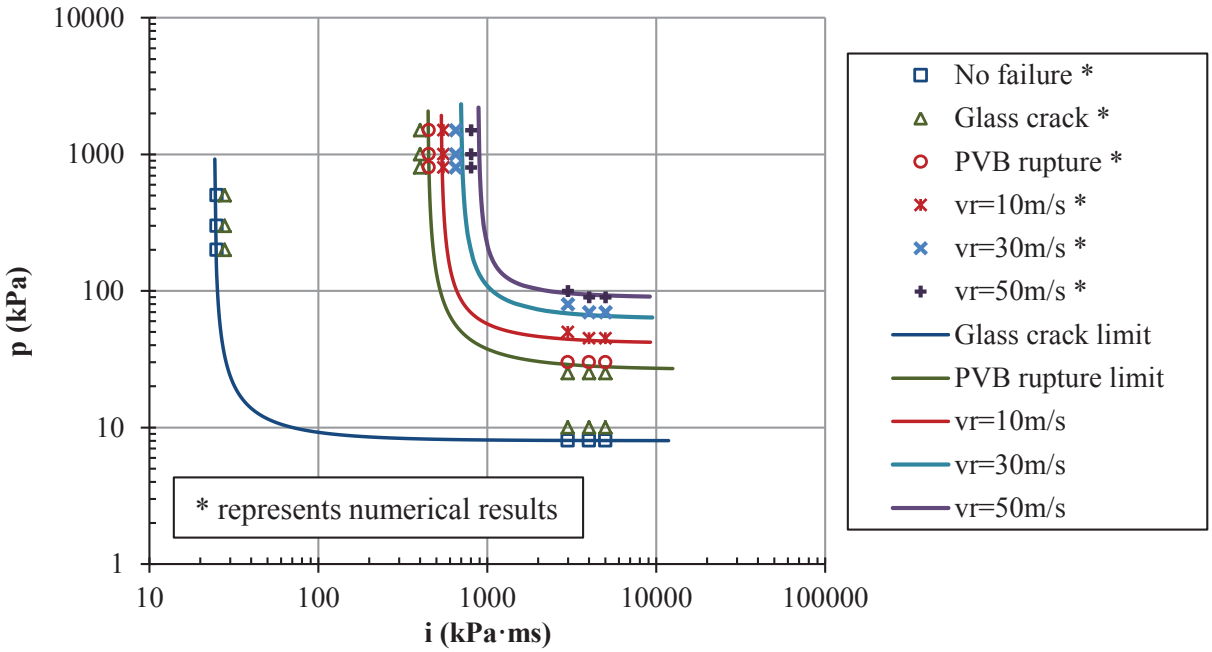

Figure 25. Comparison between the generated P-I curves and FEA results in impulsive and quasi-static regions

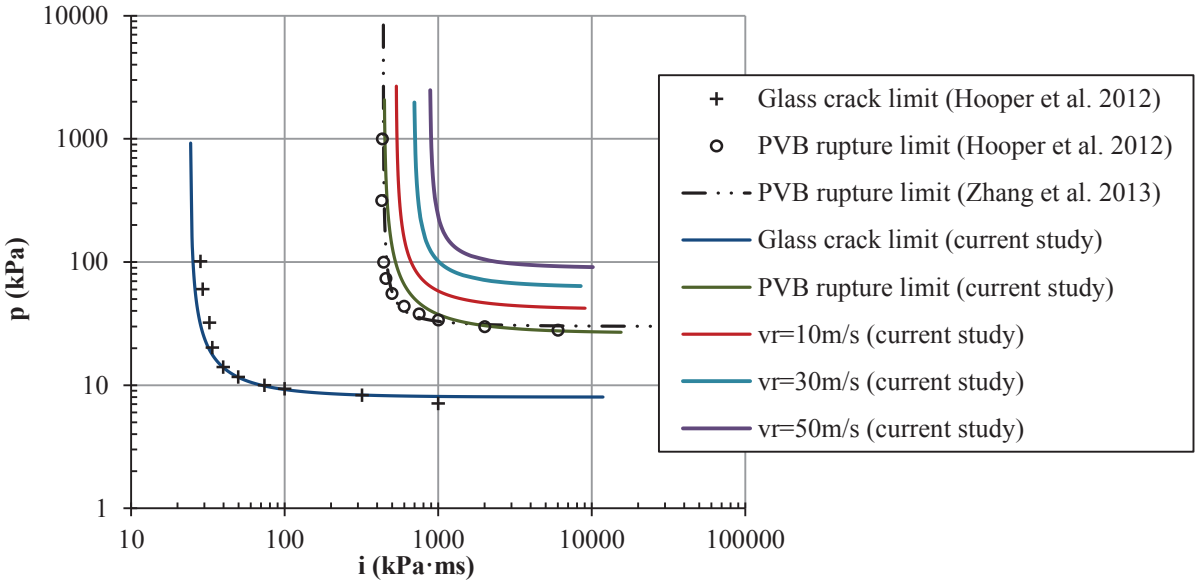

Figure 26. Comparison between the generated P-I curves and predictions from other researchers

Figure Caption List